Journal of Sound and Vibration 611 (2025) 119111

Contents lists available at ScienceDirect

Journal of Sound and Vibration

journal homepage: www.elsevier.com/locate/jsvi

Self-similar eigenvalue distribution of a binary tree-structured mass–spring–damper system

Róbert Rochlitz, Bendegúz Dezső Bak *, Tamás Kalmár-Nagy

Department of Fluid Mechanics, Faculty of Mechanical Engineering, Budapest University of Technology and Economics, Műegyetem rkp. 3., H-1111 Budapest, Hungary

ARTICLE INFO

Keywords:
MDOF linear system
Eigenvalue distribution
Devil's staircase
Mistuning

ABSTRACT

The eigenvalue distribution of a binary tree-structured multi-degree-of-freedom linear oscillator is examined. The block masses and spring stiffnesses in the model are a power-law function of the tree level. A recursive formula is proven for the characteristic polynomial of the undamped system. For the power-law quotient $\sigma = 1/2$ the resulting characteristic equation is solved analytically and the eigenvalue distribution is derived as the function of the tree level up to the limit of the infinite tree. The importance of the eigenvalue distribution is demonstrated with examples of the dynamical behavior, when the system is subjected to small mistuning of its block masses. The mistuning perturbs the block masses by drawing a random value from a uniform distribution centered around the base value of each block mass. The width of the uniform distribution for each block mass is given by the product of the base value of the mass and the mistuning parameter r. The displacement solutions of the governing differential equation with two sets of initial conditions are compared for different values of the mistuning parameter r. Even though the mistuning has only a small effect on the eigenfrequencies of the system, it is concluded that the small perturbation of the block masses can cause a significant shift in the apparent frequency of the vibration.

1. Introduction

The dynamics of vibrational systems and the associated energy transfer mechanisms are a fundamental subject of engineering research. State-of-the-art engineering systems are complex, and their study requires a certain degree of simplification. Engineering approximations and physical modeling are applied to derive mechanical models that can be studied with the tools of classical mechanics. This modeling approach often leads to a multi degree-of-freedom (MDoF) mechanical system. Linear MDoF systems are characterized by their eigenfrequencies and mode shapes, their response to combined excitations is governed by the superposition principle [1]. Consequently, the response of linear vibrational systems scales with the input energy magnitude, but the qualitative behavior remains unchanged. Energy transfer and the distribution of vibrational energy in linear systems are directly related to the mode shapes [2]. This predictability of linear systems can be exploited by using tuned mass dampers (TMD) designed to reduce vibrations within a narrow frequency range. TMDs are effective independently of the magnitude of the vibration amplitude, but their effectiveness is limited to their intended operating frequency [3,4].

In general, real life systems feature nonlinearity. While new challenges arise with the introduction of nonlinearity, it also offers new approaches to channel vibrational energy. The superposition principle does not apply for nonlinear systems. Hence, they are sensitive to the input energy, their qualitative behavior changes for increasing vibration amplitude [5]. On the other hand, nonlinear

* Corresponding author.
E-mail addresses: rochlitzr@edu.bme.hu (R. Rochlitz), bak.bendeguz@gpk.bme.hu (B.D. Bak), kalmar.nagy.tamas@gpk.bme.hu (T. Kalmár-Nagy).

https://doi.org/10.1016/j.jsv.2025.119111
Received 2 December 2024; Received in revised form 4 April 2025; Accepted 5 April 2025
Available online 20 April 2025
0022-460X/

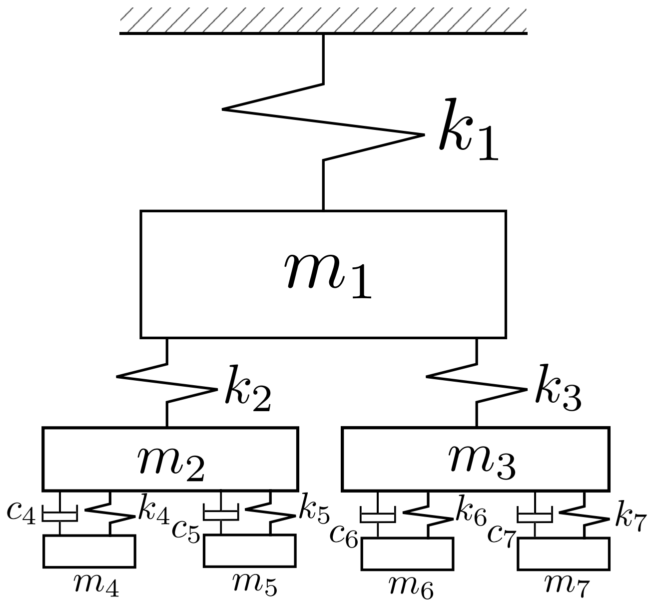

Fig. 1.1. The mechanistic turbulence model with $n = 3$ levels.

dissipative elements – often referred to as nonlinear energy sinks (NESs) – offer efficient, irreversible energy transfer and high dissipation for a broad range of vibration frequencies as opposed to TMDs. The efficacy of NESs depends on the input energy, i.e., the magnitude of the vibration amplitude. Some types of NESs require a threshold input energy to activate and their effectiveness peaks in a broad, but limited input energy range [6]. Researchers proposed a variety of NES designs to improve their effectiveness, e.g., bistable NES [7–9] and vibro-impact NES [10–12].

The real life prevalence of nonlinearity in engineering systems seemingly makes linear modeling obsolete. However, infinite DoF linear systems can also exhibit complex behavior [13]. Moreover, finite-dimensional nonlinear systems can be embedded in infinite-dimensional linear systems via the Carleman linearization technique [14]. Studying high DoF or infinite DoF linear systems can lead to intriguing findings. A typical example is self-similar systems in which parts of the system resemble the whole system. Self-similarity can be exploited to derive the eigenvalue distribution of a self-similar linear system, even in the limit of infinite DoF [15]. Nature often follows such self-similar patterns [16], understanding their advantageous properties might inspire innovations and scientific breakthroughs.

In this study a MDoF binary tree-structured linear mechanical oscillator shown in Fig. 1.1, dubbed "mechanistic turbulence model", is studied. The structure of this model is shown in the figure, the masses of blocks are connected by linear springs and also by linear dampers between the blocks of the last two levels.

Our motivation of studying this particular structure stems from our interest in the turbulent energy cascade that is sustained by the production of large vortices that eventually break up into gradually smaller vortices until viscous dissipation prevails at the smallest scales of eddies [17–19]. In the mechanistic turbulence model the blocks have decreasing masses as the bottom of the tree is approached, thus, different scales of masses make up the model. The energy of the model is dissipated by the dampers that are connected to the blocks with the smallest masses.

Kalmár-Nagy and Bak [2] studied the energy distribution among the levels/scales of the mechanistic turbulence model, a formula was derived analytically for the steadily decaying phase of the vibration, when the initial transients have already died out. They showed that for certain parametrizations the mechanistic turbulence model exhibits a mean energy distribution over the mass scales that is qualitatively similar to the Kolmogorov spectrum of 3D homogeneous isotropic turbulence [18,19]. As the eigenvalues of the system determine its dynamics, the eigenvalue distribution of the mechanistic turbulence model was also examined. The distribution of the eiqenfrequencies resembled a Devil's staircase function. The characteristic equation of the undamped model for a set of system parameters was provided as a claim. Zanette [20] also studied energy exchange between coupled linear oscillators.

Vakakis et al. [5] discusses that the introduction of strong, essential nonlinearities gives rise to targeted energy transfer in MDoF vibrational systems. They show various examples for systems that consist of a primary MDoF linear oscillator to which one or multiple nonlinear attachments, NESs are connected. These NESs realize irreversible, efficient energy transfer from the primary linear system towards the nonlinear attachments. Nonlinear systems that involve multiple scales (for instance, the mechanistic turbulence model) can exhibit an energy cascade, i.e., a primarily one-way transfer of energy from the larger scales towards the smaller ones. This is referred to as "mechanical turbulence" [21–23].

In another study, Bak et al. [24] added essential nonlinearity to the mechanistic turbulence model to initiate efficient, irreversible energy transfer for different types of external excitations. The dynamics of such nonlinear oscillators are dominated by the nonlinear normal modes that are commonly visualized with the frequency energy plot. Finding these nonlinear normal modes and the construction of the frequency energy plot require the calculation of the eigenvalues of the two underlying linear systems. The nonlinear connections are either completely omitted or replaced with rigid connections to derive these underlying linear systems. This led us back to further study the purely linear mechanistic turbulence model, particularly focusing on the eigenvalue distribution of the model.

Eigenvalue distribution of various structures is also frequently studied with self-similar matrices and graphs cropping up in diverse areas. Xiuqing and Youyan [25] and Fu et al. [26] studied one-dimensional Fibonacci-class quasilattices and showed that for these types of lattices the energy spectrum exhibits a staircase behavior. He et al. [27] studied a family of tree graphs whose adjacency matrix also approaches a piecewise constant Cantor function as the tree grows. Kalmár-Nagy et al. [15] considered the adjacency matrix associated with a graph that describes transitions between the states of the discrete Preisach memory model. The characteristic polynomial of the adjacency matrix was shown to be the product of Chebyshev polynomials. The eigenvalue distribution was explicitly calculated and was shown to approach a scaled Devil's staircase. Loong et al. [28] analyzed mechanical oscillators that have fractal monopodial tree structure. They provided analytical formulas for the eigenfrequencies and mode shapes of the self-similar structure. While this study did not particularly focus on the eigenfrequency distribution of the system, the high geometric multiplicity of some vibration modes suggest that the eigenvalue distribution might form a Cantor function in the limiting case of an infinite tree. The authors also highlighted the practicality of the particular structure as it efficiently reduces the vibration amplitude of the main trunk.

Kostadinov [29] expressed the free energy of a one-dimensional Ising model with random couplings in terms of the maximal eigenvalue of a self-similar matrix. He also related the calculation for the spectra of molecular type of systems in the tight binding approximation to the eigenvalues and eigenvectors of self-similar Hermitian matrices. Stosic et al. [30] found the analytical expression for the residual entropy of the two-dimensional Ising model with nearest-neighbor antiferromagnetic coupling in terms of the fractal Fibonacci matrix. Katsanos and Evangelou [31] studied the level-spacing distribution of a fractal Fibonacci matrix to address questions related to Anderson localization and quantum chaos. Hsu et al. introduced Fibonacci cubes as a new class of self-similar graphs [32]. Ferrand [33] considered a self-similar matrix related to the Thue–Morse sequence.

The goal of this paper is to describe and formally prove some of these properties in the case of the mechanistic turbulence model (for example, we show that the mechanistic turbulence model of Fig. 1.1 has a self-similar eigenvalue distribution in the limit of infinite DoFs), offering an example of analytical treatment of a self-similar graph to the wider scientific community. We provide the characteristic polynomial of the undamped mechanistic turbulence model with proof for a more general set of system parameters than those reported in [2]. For a specific choice of the parameter σ introduced by Eq. (2.5) an analytical formula is also derived for the eigenfrequencies of the system. This closed form analytical formula allows us to prove that the eigenvalue distribution of the system is a scaled Devil's staircase function. The significance of the eigenvalue distribution on the dynamical behavior of the system is demonstrated through a set of examples, in which small perturbations are applied to the block masses of the mechanistic turbulence model.

This paper is structured as follows. In Section 2 the mechanistic turbulence model is introduced. In Section 3 analytical results regarding the eigenvalue distribution of the mechanistic turbulence model are derived. A formula for the characteristic polynomial of the undamped system is given. Then, a closed form analytical expression is provided for the undamped system, when $\sigma = 1/2$. It is proven that the eigenvalue distribution of the undamped system follows a Devil's staircase function, in particular, the corresponding Devil's staircase function is formulated for both finite and infinite DoF systems. In Section 3.4 another formula is provided for the characteristic equation of the grounded variant of the undamped system that was first proposed without a proof by Kalmár-Nagy and Bak [2]. In Section 4 mistuning of the model parameters is introduced, in particular, a perturbation to the masses of the blocks is applied. Preliminary numerical results of the eigenvalue distribution of the unperturbed and perturbed systems are presented. In Section 5 the effect of the mistuning on the dynamics of the system is discussed. Finally, conclusions are drawn in Section 6.

2. Model description

2.1. The mechanistic turbulence model

The mechanistic turbulence model depicted in Fig. 1.1 is an n-level binary tree-structured linear mechanical oscillator that is described by the set of differential equations

$$\begin{aligned}
m_i\ddot{x}_i &= -k_i x_i + k_{2i}(x_{2i} - x_i) + k_{2i+1}(x_{2i+1} - x_i), \quad i \in \mathcal{I}(1),\\
m_i\ddot{x}_i &= k_i(x_{\lfloor i/2 \rfloor} - x_i) + k_{2i}(x_{2i} - x_i) + k_{2i+1}(x_{2i+1} - x_i), \quad i \in \mathcal{I}(l),\ l = 2, \dots, n-2,\\
m_i\ddot{x}_i &= k_i(x_{\lfloor i/2 \rfloor} - x_i) + k_{2i}(x_{2i} - x_i) + k_{2i+1}(x_{2i+1} - x_i) + c_{2i}(\dot{x}_{2i} - \dot{x}_i)\\
&\quad + c_{2i+1}(\dot{x}_{2i+1} - \dot{x}_i), \quad i \in \mathcal{I}(n-1),\\
m_i\ddot{x}_i &= k_i(x_{\lfloor i/2 \rfloor} - x_i) + c_i(\dot{x}_{\lfloor i/2 \rfloor} - \dot{x}_i) \quad i \in \mathcal{I}(n),
\end{aligned} \tag{2.1}$$

where m_i are the masses of the blocks, k_i are the stiffnesses of the springs, c_i are the damping coefficients of the dampers, $x_i \equiv x_i(t)$ are the displacements of the blocks, and t is the time. The set of indices $\mathcal{I}(l) = \left\{2^{l-1}, \dots, 2^l - 1\right\}$ covers the indices of all elements on level l.

In this model, the blocks of masses are connected by linear springs. Linear dampers are only introduced between the blocks of the last two levels as Fig. 1.1 shows.

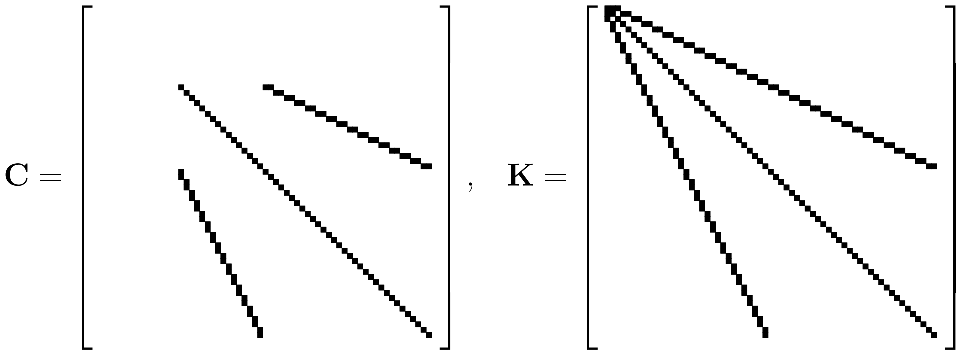

Fig. 2.1. The structure of the damping and the stiffness matrices for $n = 6$ levels, the black squares show the nonzero elements.

The system of differential equations (2.1) can be formulated in matrix form as

$$\mathbf{M}\ddot{\mathbf{x}}(t) + \mathbf{C}\dot{\mathbf{x}}(t) + \mathbf{K}\mathbf{x}(t) = \mathbf{0}, \tag{2.2}$$

where $\mathbf{M}$, $\mathbf{C}$, and $\mathbf{K}$ are the mass, damping, and stiffness matrices, respectively. Let $N = 2^n - 1$ be the number of degrees of freedom in the system. Then, the diagonal mass matrix $\mathbf{M}$ has the form

$$\mathbf{M} = \operatorname{diag}(m_1, \dots, m_N). \tag{2.3}$$

Examples of matrices $\mathbf{C}$ and $\mathbf{K}$ for $n = 3$ levels are given in Eq. (2.4), and their structure is shown in Fig. 2.1 for $n = 6$ levels. The damping matrix $\mathbf{C}$ has a zero submatrix in its top left corner for $n \geq 3$, because dampers are placed exclusively between the blocks of the last two levels.

$$\begin{gathered}
\mathbf{C} = \begin{bmatrix} 0 & 0 & 0 & 0 & 0 & 0 & 0 \\ 0 & c_4 + c_5 & 0 & -c_4 & -c_5 & 0 & 0 \\ 0 & 0 & c_6 + c_7 & 0 & 0 & -c_6 & -c_7 \\ 0 & -c_4 & 0 & c_4 & 0 & 0 & 0 \\ 0 & -c_5 & 0 & 0 & c_5 & 0 & 0 \\ 0 & 0 & -c_6 & 0 & 0 & c_6 & 0 \\ 0 & 0 & -c_7 & 0 & 0 & 0 & c_7 \end{bmatrix} \\
\mathbf{K} = \begin{bmatrix} k_1 + k_2 + k_3 & -k_2 & -k_3 & 0 & 0 & 0 & 0 \\ -k_2 & k_2 + k_4 + k_5 & 0 & -k_4 & -k_5 & 0 & 0 \\ -k_3 & 0 & k_3 + k_6 + k_7 & 0 & 0 & -k_6 & -k_7 \\ 0 & -k_4 & 0 & k_4 & 0 & 0 & 0 \\ 0 & -k_5 & 0 & 0 & k_5 & 0 & 0 \\ 0 & 0 & -k_6 & 0 & 0 & k_6 & 0 \\ 0 & 0 & -k_7 & 0 & 0 & 0 & k_7 \end{bmatrix}
\end{gathered} \tag{2.4}$$

2.2. Model parameters

The block masses m_i and the spring stiffnesses k_i of the model are considered to follow a simple power-law, where the parameters on a given level l are the same. In other words, each level is described by a mass scale M_l and a stiffness scale K_l as

$$\begin{aligned} m_i &= M_l = \sigma^{1-l}, \qquad i \in \mathcal{I}(l), \quad l = 1, \dots, n, \\ k_i &= K_l = \sigma^{1-l}, \qquad i \in \mathcal{I}(l), \quad l = 1, \dots, n, \end{aligned} \tag{2.5}$$

where parameter $\sigma \geq 0$ is the base of the power-law distribution. This equation prescribes the mass of the first (top), largest block to be $M_1 = 1$, and the stiffness of the spring connecting it to the motionless wall to be $K_1 = 1$.

Each damper in the last level has the same damping coefficient, i.e.,

$$c_i = C_n \geq 0, \qquad i \in \mathcal{I}(n). \tag{2.6}$$

3. Eigenvalues and eigenvalue distribution of the mechanistic turbulence model

For the undamped system ($C_n = 0$) all eigenvalues of system (2.1) are purely imaginary. The top left plot in Fig. 3.1 shows the imaginary parts of the eigenvalues for $n = 6$ levels and $\sigma = 1/2$. We call this ordered set of the imaginary parts of the eigenvalues

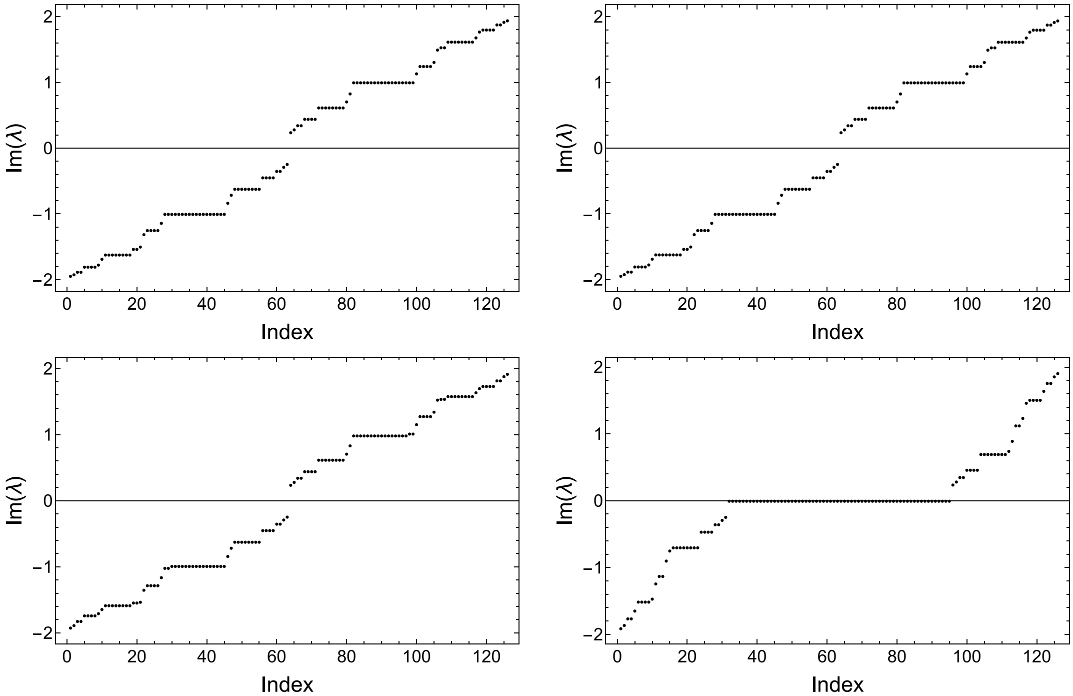

Fig. 3.1. Eigenvalue distribution of the undamped system (top left), $C_n = 0.001$ (top right), $C_n = 0.01$ (bottom left), and $C_n = 0.125$ (bottom right). The system has $n = 6$ levels and $\sigma = 1/2$.

the *eigenvalue distribution*. This eigenvalue distribution resembles the Devil's staircase, a notion that will be made precise and proven in Section 3.3. The eigenvalue distributions for positive values of the damping $C_6 = 0.001, \ldots, 0.125$ are also shown in Fig. 3.1.

Kalmár-Nagy and Bak [2] provided – without proof – an analytic formula for the characteristic polynomial of the grounded mechanistic turbulence model (additional $n+1$th level springs grounded the blocks in the nth level) with a set of parameters obeying the scaling relation (2.5). Their formula contained Chebyshev polynomials of the second kind. The appearance of Chebyshev polynomials in the characteristic function is not surprising, since characteristic functions of tridiagonal and other structured matrices frequently involve Chebyshev polynomials.

Let us denote by $U_l(\lambda)$ the Chebyshev polynomial of the second kind of degree l [34]. For example, they can be defined by the recursive relations

$$U_0(\lambda) = 1; \quad U_1(\lambda) = 2\lambda; \quad U_{l+1}(\lambda) = 2\lambda\, U_l(\lambda) - U_{l-1}(\lambda), \tag{3.1}$$

or by the explicit formula

$$U_l(\cos(y)) = \frac{\sin((l+1)y)}{\sin y}. \tag{3.2}$$

3.1. Characteristic polynomial of the mechanistic turbulence model

The equation of motion of the undamped ($C_n = 0$) system (2.1) with parameters specified by the power law in Eq. (2.5) reduces to

$$\begin{aligned}
&M_l\ddot{x}_i = \sigma K_l x_{2i} + \sigma K_l x_{2i+1} - (1+2\sigma)K_l x_i, \quad i \in \mathcal{I}(l),\ l = 1,\\
&M_l\ddot{x}_i = K_l x_{\lfloor i/2 \rfloor} + \sigma K_l x_{2i} + \sigma K_l x_{2i+1} - (1+2\sigma)K_l x_i, \quad i \in \mathcal{I}(l),\ l = 2, \ldots, n-1,\\
&M_l\ddot{x}_i = K_l x_{\lfloor i/2 \rfloor} - K_l x_i, \quad i \in \mathcal{I}(l),\ l = n,
\end{aligned} \tag{3.3}$$

with $M_1 = 1$, $K_1 = 1$.

Let $\mathbf{M}_n$ and $\mathbf{K}_n$ be the mass and stiffness matrices described by Eq. (3.3) of the mechanistic turbulence model depicted in Fig. A.1, where the subscript n stands for the number of tree levels.

Let $\mathbf{A}_n(\lambda)$ be

$$\mathbf{A}_n(\lambda) = \lambda^2\mathbf{M}_n + \mathbf{K}_n, \tag{3.4}$$

then the characteristic equation of system (3.3) is

$$\det\left(\mathbf{A}_n(\lambda)\right) = 0. \tag{3.5}$$

Theorem 1. *The characteristic polynomial of the system described by Eq. (3.3) has the form*

$$\begin{aligned} \det(\mathbf{A}_n(\lambda)) &= \sigma^{2+(n-2)2^n} P_n(\lambda), \\ P_n(\lambda) &= \frac{Q_n(\lambda)}{Q_{n-1}(\lambda)} P_{n-1}^2(\lambda), \end{aligned} \tag{3.6}$$

where

$$\begin{aligned} P_0(\lambda) &= Q_0(\lambda) = 1, \\ Q_n(\lambda) &= q^n U_n\left(\frac{\lambda^2+a}{b}\right) - 2\sigma K_1 q^{n-1} U_{n-1}\left(\frac{\lambda^2+a}{b}\right), \\ a &= \frac{K_1}{M_1}(1+2\sigma), \quad b = \frac{2K_1}{M_1}\sqrt{2\sigma}, \quad q = K_1\sqrt{2\sigma}, \end{aligned} \tag{3.7}$$

and U_n are Chebyshev polynomials of the second kind.

The proof of this theorem is provided in Appendix A. We immediately have the following

Corollary 1. *The polynomial $P_n(\lambda)$ in Eq. ((3.6)) can be written as*

$$P_n(\lambda) = Q_n(\lambda)\prod_{l=0}^{n-1} P_l(\lambda), \quad n \geq 1. \tag{3.8}$$

Proof. We see that $P_1(\lambda) = Q_1(\lambda) = M_1\lambda^2 + K_1$, thus Eq. (3.8) holds for $P_1(\lambda)$. Next we assume that it holds up to $n-1$, $n \geq 2$, then for n we have

$$P_n(\lambda) = \frac{Q_n(\lambda)}{Q_{n-1}(\lambda)} P_{n-1}^2(\lambda) = \frac{Q_n(\lambda)}{Q_{n-1}(\lambda)} P_{n-1}(\lambda) \cdot Q_{n-1}(\lambda)\prod_{l=0}^{n-2} P_l(\lambda) = Q_n(\lambda)\prod_{l=0}^{n-1} P_l(\lambda). \quad \square \tag{3.9}$$

Consequently we obtain

Corollary 2. *The polynomial $P_n(\lambda)$ in Eq. ((3.6)) can be written as*

$$P_n(\lambda) = Q_n(\lambda)\prod_{l=0}^{n-1} Q_{n-1-l}^{2^l}(\lambda), \quad n \geq 1. \tag{3.10}$$

Proof. Eq. (3.10) clearly holds for $P_1(\lambda)$. Assuming it holds up to some $n-1$, $n \geq 2$, for n we have

$$\begin{aligned} P_n(\lambda) &= \frac{Q_n(\lambda)}{Q_{n-1}(\lambda)} P_{n-1}^2(\lambda) = \frac{Q_n(\lambda)}{Q_{n-1}(\lambda)} Q_{n-1}^2(\lambda)\prod_{l=0}^{n-2} Q_{n-2-l}^{2^{l+1}}(\lambda) \\ &= Q_n(\lambda)Q_{n-1}(\lambda)\prod_{l=1}^{n-1} Q_{n-1-l}^{2^l}(\lambda) = Q_n(\lambda)\prod_{l=0}^{n-1} Q_{n-1-l}^{2^l}(\lambda). \end{aligned} \quad \square \tag{3.11}$$

Based on Corollary 2., the first few characteristic polynomials $P_n(\lambda)$ are

$$\begin{aligned} P_1(\lambda) &= Q_1(\lambda), \\ P_2(\lambda) &= Q_1(\lambda)Q_2(\lambda), \\ P_3(\lambda) &= Q_1^2(\lambda)Q_2(\lambda)Q_3(\lambda), \\ P_4(\lambda) &= Q_1^4(\lambda)Q_2^2(\lambda)Q_3(\lambda)Q_4(\lambda), \\ P_5(\lambda) &= Q_1^8(\lambda)Q_2^4(\lambda)Q_3^2(\lambda)Q_4(\lambda)Q_5(\lambda), \\ P_6(\lambda) &= Q_1^{16}(\lambda)Q_2^8(\lambda)Q_3^4(\lambda)Q_4^2(\lambda)Q_5(\lambda)Q_6(\lambda). \end{aligned} \tag{3.12}$$

The characteristic polynomials written out in Eq. (3.12) show that system (3.3) has a large number of repeated eigenvalues, which explains the plateaus in the eigenvalue distributions shown in Fig. 3.1.

3.2. Analytical calculation of the eigenvalues

Using Eq. (3.10) it is possible to provide an analytical formula to calculate the eigenvalues of the system given by Eq. (3.3) for certain special cases. Since Eq. (3.10) shows that the characteristic polynomial $P_n(\lambda)$ is a product of the $Q_l(\lambda)$ ($l = 1, \ldots, n$) generalized Chebyshev polynomials, it is enough to find an analytical solution for the problem

$$Q_l(\lambda) = 0. \tag{3.13}$$

Written out, this is equivalent to

$$Q_l(\lambda) = q^l U_l\left(\frac{\lambda^2+a}{b}\right) - 2\sigma K_1 q^{l-1} U_{l-1}\left(\frac{\lambda^2+a}{b}\right) = 0. \tag{3.14}$$

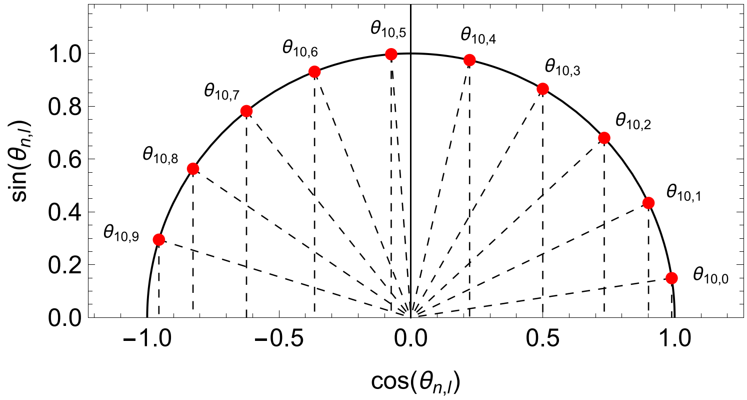

Fig. 3.2. An example of the angles $\theta_{l,j}$ defining the $\lambda_{l,j}$ roots of $Q_l(\lambda)$ of the undamped mechanistic turbulence model on the unit circle for $l = 10$, $\sigma = 1/2$.

Dividing (3.14) by q^l and remembering that $q = K_1\sqrt{2\sigma}$ (see Eq. (3.6)), we get

$$\begin{aligned} &U_l\left(\frac{\lambda^2+a}{b}\right) - \frac{2\sigma K_1}{q}U_{l-1}\left(\frac{\lambda^2+a}{b}\right) = U_l\left(\frac{\lambda^2+a}{b}\right) - \frac{2\sigma}{\sqrt{2\sigma}}U_{l-1}\left(\frac{\lambda^2+a}{b}\right) \\ &= U_l\left(\frac{\lambda^2+a}{b}\right) - \sqrt{2\sigma}U_{l-1}\left(\frac{\lambda^2+a}{b}\right) = 0. \end{aligned} \tag{3.15}$$

Let us introduce

$$\cos y = \frac{\lambda^2+a}{b}. \tag{3.16}$$

By substituting $U_l(\cos(y))$ from Eq. (3.2) and $\cos y$ from Eq. (3.16) into (3.15) (provided $\sin y \neq 0$, i.e., $y \neq \pi j$, $j \in \mathbb{Z}$) we get

$$\begin{aligned} \sin((l+1)y) - \sqrt{2\sigma}\sin(ly) &= (1+\sqrt{2\sigma})\sin\left(\frac{y}{2}\right)\cos\left(\left(l+\frac{1}{2}\right)y\right) \\ &\quad + (1-\sqrt{2\sigma})\cos\left(\frac{y}{2}\right)\sin\left(\left(l+\frac{1}{2}\right)y\right) = 0. \end{aligned} \tag{3.17}$$

For the special case $\sigma = 1/2$ Eq. (3.17) reduces to

$$\sin\left(\frac{y}{2}\right)\cos\left(\left(l+\frac{1}{2}\right)y\right) = 0, \tag{3.18}$$

whose solutions are

$$y = \begin{cases} 2\pi j, & j \in \mathbb{Z}, \\ \frac{2j+1}{2l+1}\pi, & j \in \mathbb{Z}. \end{cases} \tag{3.19}$$

With the constraint $y \neq \pi j$, $j \in \mathbb{Z}$ that is required by the substitution of $U_l(\cos(y))$ performed in Eq. (3.17), the eigenvalues are

$$\lambda_{l,j} = \pm\sqrt{b\cos(y)-a} = \pm\sqrt{b\cos\left(\frac{2j+1}{2l+1}\pi\right)-a}, \quad j = 0,\dots,l-1. \tag{3.20}$$

Note that $a, b > 0$ and

$$a - b = \frac{K_1}{M_1}\left(1-\sqrt{2\sigma}\right)^2 \geq 0, \tag{3.21}$$

thus the eigenvalues only have imaginary parts and can be written as

$$\lambda_{l,j} = \pm\imath\sqrt{a - b\cos\left(\frac{2j+1}{2l+1}\pi\right)} = \pm\imath\sqrt{a-b\cos(\theta_{l,j})}, \quad j = 0,\dots,l-1. \tag{3.22}$$

Fig. 3.2 shows the angles $\theta_{l,j}$ defining the eigenvalues of the mechanistic turbulence model on the unit circle.

3.3. Eigenvalue distribution

Spectral properties of structured matrices have been extensively studied. The book by Böttcher and Grudsky [35] focuses on banded Toeplitz matrices. Spectral graph theory (see, for example, [36]) relates the eigenvalues of the adjacency matrix to other properties of the graph. In the following derivations we assume that the scaling parameter of Eq. (2.5) is $\sigma = 1/2$. Then, we can exploit the findings of Section 3.2 to demonstrate that the eigenvalue distribution follows a Devil's staircase function. We also derive the Devil's staircase function in the limit of $n \to \infty$.

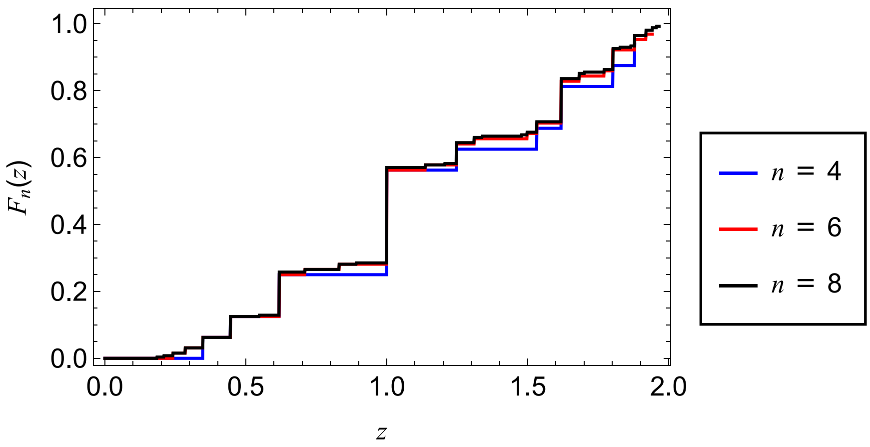

Fig. 3.3. Eigenvalue distribution function for the undamped mechanistic turbulence model for different number of levels n, $\sigma = 1/2$.

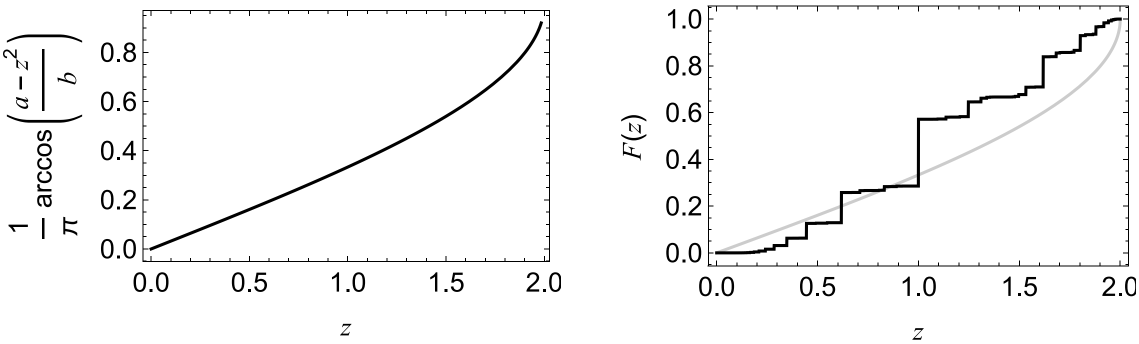

Fig. 3.4. Transformation between the distribution function $F_n(z)$ and $h_n(z)$ (left), and the limit distribution function $F(z)$ (right).

Based on Eq. (3.22) for any $l \in \{1, \dots, n\}$ the solutions of $Q_l(\lambda) = 0$ have the form

$$\lambda_{l,j} = \pm\imath\sqrt{a - b\cos\left(\frac{2j+1}{2l+1}\pi\right)}, \quad j = 0, \dots, l-1. \tag{3.23}$$

According to Eq. (3.6) we have $a = b = 2K_1/M_1$.

Let $F_n(z)$ be the distribution function of positive eigenfrequencies as

$$F_n(z) = \frac{\#\left\{\lambda : \det(\lambda^2\mathbf{M}_n + \mathbf{K}_n) = 0,\ 0 < \mathrm{Im}(\lambda) \le z\right\}}{2^n}, \tag{3.24}$$

where # denotes the number of elements in a set. The $F_n(z)$ function is shown in Fig. 3.3 for a few particular values of n. Furthermore, let $h_n(z)$ be

$$h_n(z) = \frac{\#\left\{\lambda : \frac{\det(\lambda^2\mathbf{M}_n+\mathbf{K}_n)}{Q_n(\lambda)} = 0,\ 0 < \mathrm{Im}(\lambda) \le \sqrt{a - b\cos(z\pi)}\right\}}{2^n}. \tag{3.25}$$

Theorem 2. *For any $n \ge 2$, $z \in [0, \sqrt{a+b}]$ pair, the function $h_n(z)$ defined by Eq. (3.25), and the distribution function $F_n(z)$ given by Eq. (3.24) corresponding to the characteristic polynomial $P_n(\lambda) = \det(\lambda^2\mathbf{M}_n + \mathbf{K}_n)$ of system (3.3) with $\sigma = 1/2$ satisfy the relationship*

$$h_n\left(\frac{1}{\pi}\arccos\left(\frac{a-z^2}{b}\right)\right) \le F_n(z) \le h_n\left(\frac{1}{\pi}\arccos\left(\frac{a-z^2}{b}\right)\right) + \frac{n}{2^n}. \tag{3.26}$$

The proof of this theorem is provided in Appendix B.

We define the distribution function in the limit $n \to \infty$ as

$$F(z) = \lim_{n\to\infty} F_n(z). \tag{3.27}$$

Fig. 3.4 shows the transformation connecting $F_n(z)$ and $h_n(z)$ as described by Theorem 2, and the behavior of $F(z)$.

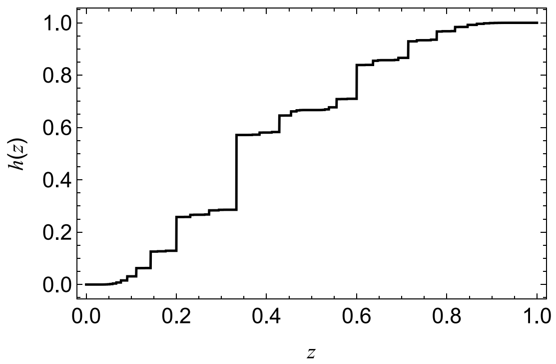

Fig. 3.5. The Devil's staircase function $h(z)$.

Kalmár-Nagy et al. [15] showed that the distribution function of the eigenvalue distribution of a similarly structured system in the limit $n \to \infty$ is closely related to the Devil's staircase function

$$g(z) = \sum_{j=1}^{\infty} \frac{\lfloor jz \rfloor}{2^j}, \qquad 0 \le z < 1. \tag{3.28}$$

Here, we consider the related function

$$h(z) = \sum_{j=1}^{\infty} \frac{1}{2^j} \left\lfloor \frac{(2j-1)z+1}{2} \right\rfloor, \qquad 0 \le z < 1, \tag{3.29}$$

which is shown in Fig. 3.5.

Theorem 3. *The distribution function $F_n(z)$ given by Eq. (3.24) corresponding to the characteristic polynomial $P_n(\lambda) = \det(\lambda^2 \mathbf{M}_n + \mathbf{K}_n)$ of system (3.3) with $\sigma = 1/2$ satisfies the relationship*

$$F(z) = \lim_{n\to\infty} F_n(z) = h\left(\frac{1}{\pi} \arccos\left(\frac{a-z^2}{b}\right)\right), \tag{3.30}$$

where $z \in [0, \sqrt{a+b})$, and $h(z)$ is defined in Eq. (3.29).

The proof of this theorem can be found in Appendix B.

Theorems 2 and 3 demonstrate that the eigenvalue distribution (top left plot of Fig. 3.1) of the undamped system is directly related to the Devil's staircase function given in Eq. (3.29).

3.4. Characteristic polynomial of the grounded mechanistic turbulence model

Kalmár-Nagy and Bak [2] provided – without proof – an analytic formula (the claim is given by Eqs. (5) and (6) in Section 3 of [2]) for the characteristic polynomial of the grounded mechanistic turbulence model (additional $n+1$th level springs grounded the blocks in the nth level) with a set of parameters obeying the scaling relation (2.5). The formula was restricted to the undamped system with $\sigma = 1/2$. Here we supply the formal proof for the recursive formula of the characteristic polynomial proposed in that earlier paper.

Similarly to Section 3.1, the damping of the system is neglected, and the masses and spring stiffnesses follow the scaling relation given in Eq. (2.5). With this, the stiffness of the springs connecting the blocks of the last level to the ground is

$$K_{n+1} = \sigma K_n. \tag{3.31}$$

The equation of motion for this grounded system with parameters following Eqs. (2.5) and (3.31) is

$$\begin{aligned}
&M_l \ddot{x}_i = \sigma K_l x_{2i} + \sigma K_l x_{2i+1} - (1+2\sigma) K_l x_i, \quad i \in \mathcal{I}(l),\ l = 1,\\
&M_l \ddot{x}_i = K_l x_{\lfloor i/2 \rfloor} + \sigma K_l x_{2i} + \sigma K_l x_{2i+1} - (1+2\sigma) K_l x_i, \quad i \in \mathcal{I}(l),\ l = 2, \dots, n-1,\\
&M_l \ddot{x}_i = K_l x_{\lfloor i/2 \rfloor} - (1+\sigma) K_l x_i, \quad i \in \mathcal{I}(l),\ l = n.
\end{aligned} \tag{3.32}$$

Theorem 4. *The characteristic polynomial of the system described by Eq. (3.32) has the form*

$$\begin{aligned}
&\det(\mathbf{A}_n(\lambda)) = \sigma^{2+(n-2)2^n} P_n(\lambda),\\
&P_n(\lambda) = \frac{Q_n(\lambda)}{Q_{n-1}(\lambda)} P_{n-1}^2(\lambda),
\end{aligned} \tag{3.33}$$

where

$$P_0(\lambda) = Q_0(\lambda) = 1,$$

$$Q_n(\lambda) = q^n U_n\left(\frac{\lambda^2+a}{b}\right) - \sigma K_1 q^{n-1} U_{n-1}\left(\frac{\lambda^2+a}{b}\right),$$

$$a = \frac{K_1}{M_1}(1+2\sigma), \quad b = \frac{2K_1}{M_1}\sqrt{2\sigma}, \quad q = K_1\sqrt{2\sigma},$$

and U_n are Chebyshev polynomials of the second kind.

The proof of this theorem is provided in Appendix C.

Remark 1. It is clear that Corollaries 1. and 2. also apply to the characteristic polynomial of the grounded system given in Eq. (3.33), since these only rely on the recursive formula of $P_n(\lambda)$, which is identical in the grounded and ungrounded cases as seen by comparing the respective Eqs. (3.6) and (3.33).

Remark 2. Note that the characteristic polynomials of the ungrounded and grounded systems given in Eqs. (3.6) and (3.33) are essentially the same, with a small difference in the factor of $U_{n-1}\left(\frac{\lambda^2+a}{b}\right)$ in the formula for $Q_n(\lambda)$. As such, the equation $Q_l(\lambda) = 0$ becomes

$$Q_l(\lambda) = q^l U_l\left(\frac{\lambda^2+a}{b}\right) - \sigma K_1 q^{l-1} U_{l-1}\left(\frac{\lambda^2+a}{b}\right) = 0. \tag{3.34}$$

Dividing this by q^l, where $q = K_1\sqrt{2\sigma}$ (given in Eq. (3.33)) yields

$$\begin{aligned} &U_l\left(\frac{\lambda^2+a}{b}\right) - \frac{\sigma K_1}{q} U_{l-1}\left(\frac{\lambda^2+a}{b}\right) = U_l\left(\frac{\lambda^2+a}{b}\right) - \frac{\sigma}{\sqrt{2\sigma}} U_{l-1}\left(\frac{\lambda^2+a}{b}\right) \\ &= U_l\left(\frac{\lambda^2+a}{b}\right) - \sqrt{\frac{\sigma}{2}} U_{l-1}\left(\frac{\lambda^2+a}{b}\right) = 0. \end{aligned} \tag{3.35}$$

This means that the derivation of the analytical eigenvalues given in Section 3.2 can be completed for the grounded mechanistic turbulence model as well, if $\sigma = 2$ is chosen.

4. Mistuning

Mistuning usually refers to variations of properties/parameters in mechanical systems, e.g., deviation in properties of turbomachinery blades caused by manufacturing imperfections, material inconsistencies, or wear. Mistuning can lead to altered resonant frequencies and amplified vibrations. In some cases mistuning is responsible for structural failures, however it can also yield increased energy transfer resulting in better energy harvesting.

Bendiksen [37,38] explored the impact of mistuning on aeroelastic stability and flutter in bladed disks. Wei and Pierre [39] presented a statistical framework for analyzing the effects of random mistiming on the forced response of nearly cyclic assemblies. Mignolet et al. [40,41] developed a combined closed-form and perturbation approach for analyzing mistuned bladed disks. Vargha [42] examined the effect of mistuning on the mechanistic turbulence model.

We consider perturbations of the masses with parameter r as

$$m_i \sim \mathcal{U}[(1-r)M_l, (1+r)M_l], \qquad i \in \mathcal{I}(l), \quad l = 1, \ldots, n, \tag{4.1}$$

where $\mathcal{U}$ denotes the continuous uniform distribution, and $r \in [0,1)$ is the mistuning parameter. We refer to the mechanistic turbulence model for $r = 0$ and $r \neq 0$ as the unperturbed system and the perturbed system, respectively. Fig. 4.1 shows typical eigenvalue distributions for increasing mistuning parameter r. The changes are typical for damped systems in the investigated range of dampings $C_n \in [0.001, 0.125]$.

As the mistuning parameter r increases, the horizontal lines of the eigenvalue distribution become slanted which means that the repeated eigenvalues break up to separate values. Adjacent non-equal eiqenfrequencies are drawn closer to each other, further smoothing this eigenspectrum.

We examined the effects of the mistuning of block masses for the complete range $r \in [0,1)$ of the mistuning parameter as well. Fig. 4.2 shows the behavior of these eigenfrequencies as a function of r for the undamped perturbed system averaged over 1000 realizations. This figure shows that the smaller eigenvalues experience smaller changes, while the largest eigenvalues increase progressively with the increase of the mistuning parameter r.

Looking at the eigenvalues $|\lambda_i|$ in increasing order, for instance, at $r = 0.99$ we find one among the ten smallest eigenvalues which exceeds $\sim 10\%$ of relative change compared to its value in the unperturbed system. On the other hand, the smallest relative difference compared to the unperturbed system among the ten largest eigenvalues is $\sim 40\%$, the largest eigenvalue $|\lambda_{63}|$ has the maximum relative change of $\sim 280\%$ from its value corresponding to the unperturbed system. This behavior of the eigenfrequencies is qualitatively the same for damped systems in the investigated range of dampings $C_n \in [0.001, 0.125]$.

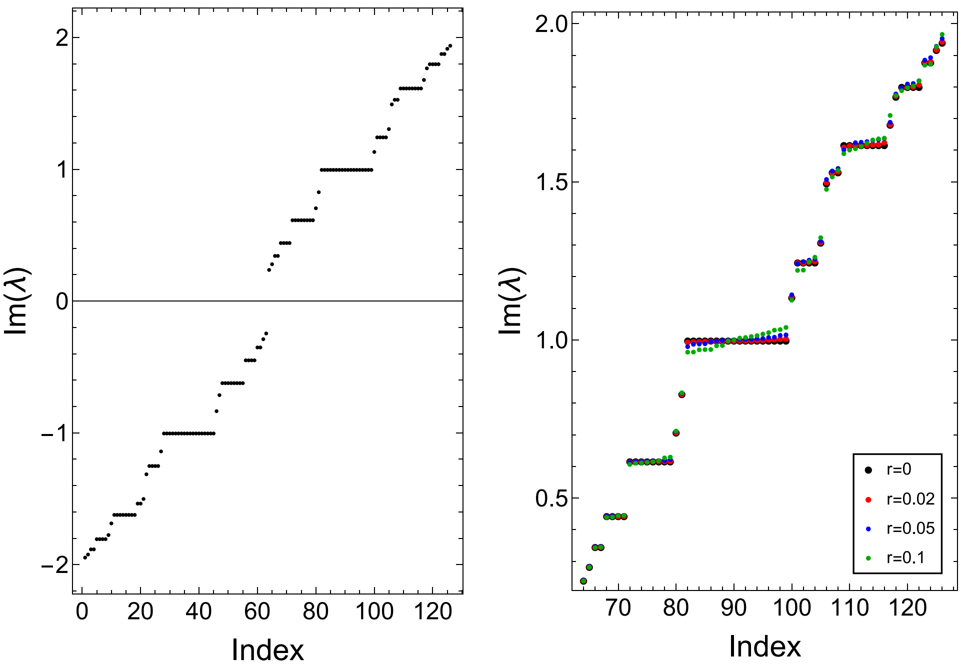

Fig. 4.1. Imaginary part of the eigenvalues for the unperturbed system (left), and for different values of the mistuning parameter r (right) without damping ($C_n = 0$).

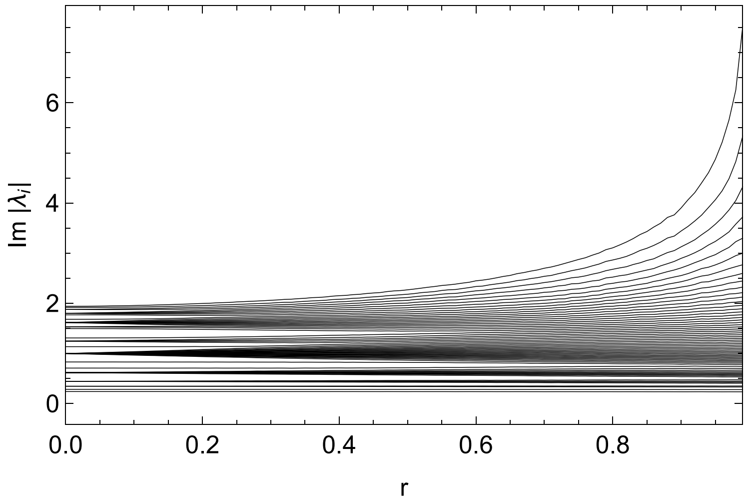

Fig. 4.2. Mean eigenvalues for $r \in [0, 1)$, averaged over 1000 realizations of the undamped perturbed system with $n = 6$ levels, $\sigma = 1/2$.

5. Dynamics

In this section, we present some results on the dynamics of the mechanistic turbulence model described in Section 2. We focus on the comparison of the unperturbed and perturbed systems to show the effect of mistuning on the dynamics. As discussed in Section 4, the mistuning breaks up the repeated eigenvalues into simple eigenvalues and increases the larger eigenfrequencies more significantly than the smaller ones. Though the actual change of the eigenfrequencies seems small for the investigated mistuning parameter range $r \in (0, 0.1]$, the oscillations are significantly affected due to the beating phenomenon that is very sensitive to small changes in the eigenfrequencies.

Let us consider a system with $n = 6$ levels, the scaling parameter of Eq. (2.5) is $\sigma = 1/2$. For $n = 6$ we have $N = 2^6 - 1 = 63$ blocks in the system. The damping coefficient of the dampers in the last level is set to $C_6 = 0.001$ to include a light damping that does not alter the eigenfrequencies significantly as shown by comparing the plots in Fig. 3.1. The moderately small mistuning parameters $r = 0.02,\ 0.05,\ 0.1$ were set.

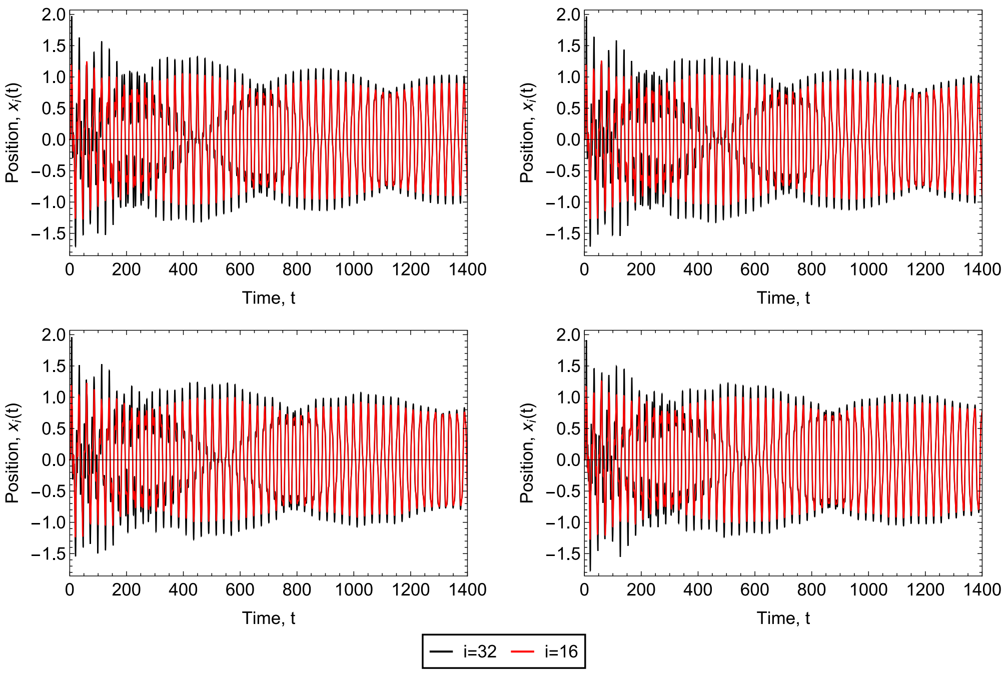

Fig. 5.1. Displacement solutions of the 16th and 32nd blocks with initial conditions (5.1) and (5.3) for the unperturbed system (top left), for $r = 0.02$ (top right), for $r = 0.05$ (bottom left), and for $r = 0.1$ (bottom right).

We consider two different sets of initial conditions (ICs) for the velocity of the blocks $i \in \{1, \ldots, 63\}$ as listed in Eqs. (5.1), (5.2), and (5.3). These equations show that only the top three blocks have a nonzero velocity $v > 0$.

- Case 1:

$$\begin{aligned} \dot{x}_i(0) &= v, \quad i = 1, 2, 3, \\ \dot{x}_i(0) &= 0, \quad i = 4, \ldots, 63. \end{aligned} \tag{5.1}$$

- Case 2:

$$\begin{aligned} \dot{x}_i(0) &= v, \quad i = 1, 2, \\ \dot{x}_i(0) &= -v, \quad i = 3, \\ \dot{x}_i(0) &= 0, \quad i = 4, \ldots, 63. \end{aligned} \tag{5.2}$$

- The initial position of every block is zero for both cases, i.e.,

$$x_i(0) = 0, \quad i = 1, \ldots, 63. \tag{5.3}$$

The total energy $E(t)$ of the system is

$$E(t) = \dot{\mathbf{x}}(t)^{\mathrm{T}} \mathbf{M} \dot{\mathbf{x}}(t) + \mathbf{x}(t)^{\mathrm{T}} \mathbf{K} \mathbf{x}(t). \tag{5.4}$$

The positive value of v is chosen such that the initial energy ($t = 0$) of the system is $E(0) = 1$, i.e.,

$$E(0) = \frac{1}{2} \left(m_1 + m_2 + m_3 \right) v^2 = 1. \tag{5.5}$$

This yields

$$v = \sqrt{\frac{2}{m_1 + m_2 + m_3}}. \tag{5.6}$$

For the unperturbed system we get $v = 1$, since $m_1 = 1$, $m_2 = m_3 = \sigma m_1 = \frac{1}{2}$.

5.1. Case 1

In Fig. 5.1 the displacement solutions for the 16th and 32nd blocks are shown for the different values of the mistuning parameter r. As we have a MDoF system with an initial condition that cannot match any mode shapes of the system, it is expected that

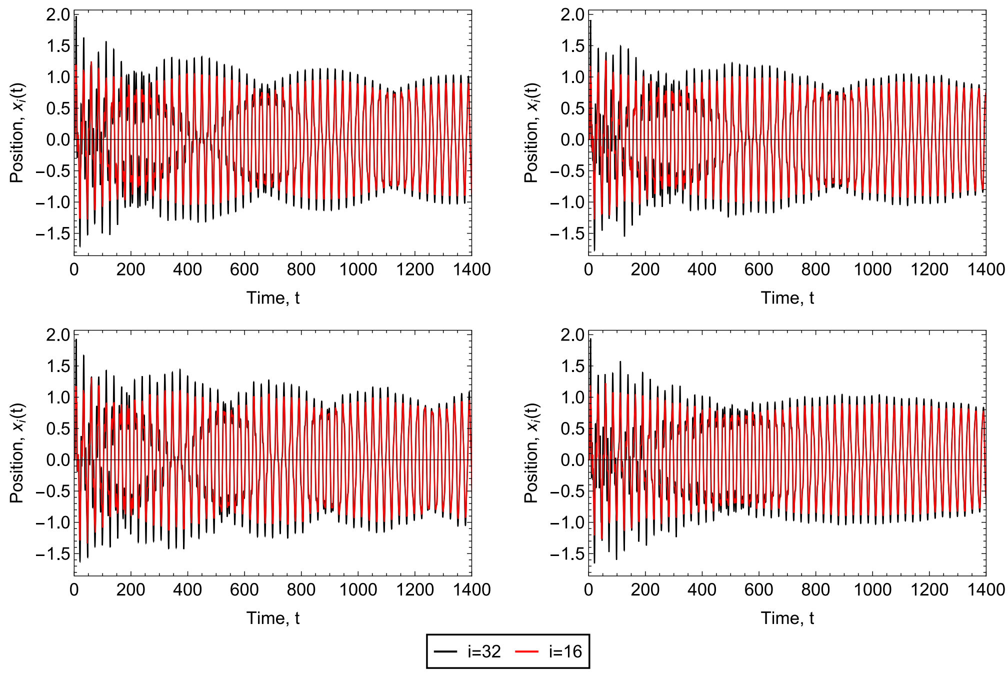

Fig. 5.2. Displacement solutions of the 16th and 32nd blocks with initial conditions (5.1) and (5.3) for the unperturbed system (top left), and for $r = 0.1$ (top right and bottom row).

Table 5.1
The dominant and the secondary frequencies of the displacement solutions of the unperturbed and perturbed systems with initial conditions (5.1) and (5.3).

Case	ω_1	ω_2	ω_1/ω_2
Unperturbed system	0.241891	0.709964	0.340708
$r = 0.02$	0.241891	0.709964	0.340708
$r = 0.05$	0.241891	0.709964	0.340708
1st realization with $r = 0.1$	0.238749	0.706823	0.337778
2nd realization with $r = 0.1$	0.241891	0.703682	0.343750
3rd realization with $r = 0.1$	0.241891	0.716247	0.337719

the displacement solutions are superpositions of multiple vibrational modes. The modulated displacement solutions shown in Fig. 5.1 agree. Introducing moderately small mistuning to the system causes the periodic behavior of the displacements to change. In particular, while the main oscillation frequency remains practically the same, the envelopes of the displacement solutions change significantly.

Since larger mistuning has a stronger impact on the dynamics of the system, we further investigated the case $r = 0.1$. Fig. 5.2 shows the displacement solutions $x_{16}(t)$ and $x_{32}(t)$ again for the unperturbed system and for three particular realizations of perturbed systems with $r = 0.1$. The larger mistuning of $r = 0.1$ permits significant shifts in the apparent frequency of the solution.

This can be explained by inspection of the energy spectral density of the displacement solution. For example, the energy spectral densities of $x_{32}(t)$ are depicted in Fig. 5.3 for the displacement solutions shown in Fig. 5.1. The two dominant eigenfrequencies (characterized by the largest peaks in Fig. 5.3) are given in Table 5.1 for the cases depicted in Figs. 5.1 and 5.2.

The dominant frequency is hardly affected by the mistuning, but the secondary frequency is significantly changed for the different realizations of the perturbed system with $r = 0.1$. Consequently, the ratio of the dominant and secondary frequencies changes which accounts for the frequency change of the apparent envelope of the displacement solutions in some cases. This is in accordance with the findings of Section 4, the eigenfrequencies can shift as a result of the mistuning. In detail, the smallest eigenfrequencies are the least affected by this shift, while the largest ones experience more significant changes for an increased value of the mistuning parameter r.

In other cases of Table 5.1, when the fractions of the two dominant frequencies are the same as those of the unperturbed system, the frequency change of the apparent envelope occurs because of the additional vibration modes being activated by the mistuning. The plots of Figs. 5.3 show indeed that additional vibrational modes activate with different frequencies in the perturbed systems as r increases. Interestingly, the active modes by the unperturbed system exclusively correspond to simple eigenvalues. In contrast, the

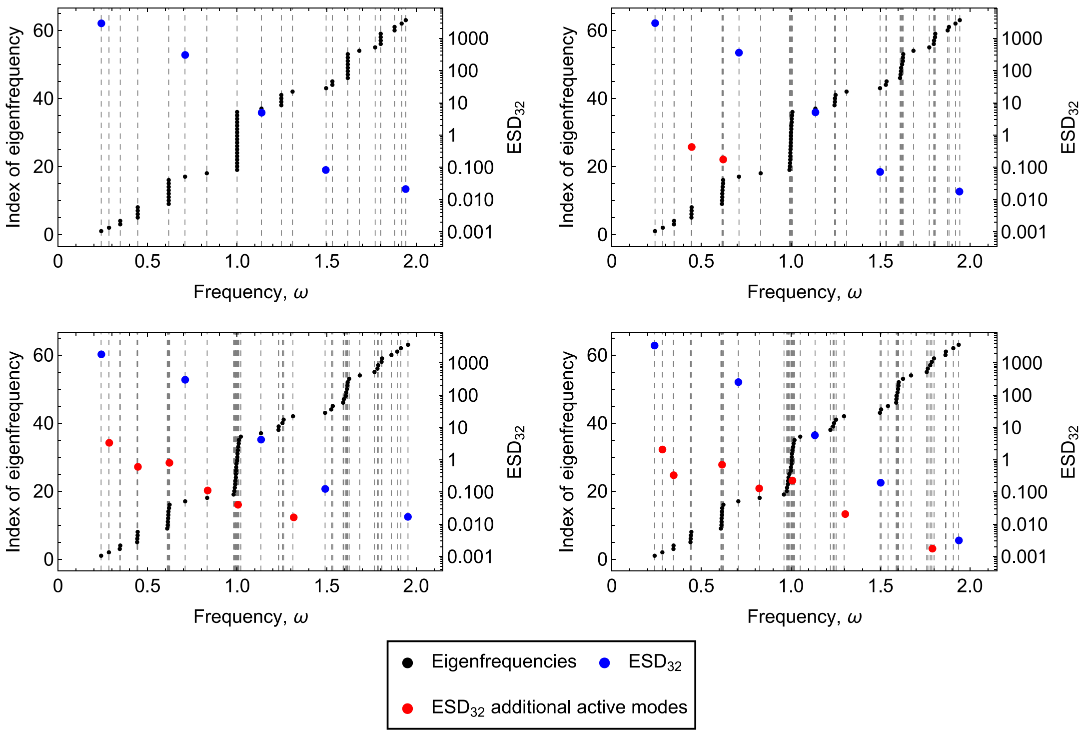

Fig. 5.3. Energy spectral density of $x_{32}(t)$ and the eigenvalue distribution of the system with initial conditions (5.1) and (5.3) for $r = 0$ (top left), for $r = 0.02$ (top right), for $r = 0.05$ (bottom left), and for $r = 0.1$ (bottom right).

Table 5.2
The dominant and the secondary frequencies of the displacement solutions of the unperturbed and perturbed systems with initial conditions (5.2) and (5.3).

Case	ω_1	ω_2	ω_1/ω_2
Unperturbed system	0.241891	0.285871	0.846154
$r = 0.02$	0.241891	0.285871	0.846154
$r = 0.05$	0.241891	0.285871	0.846154
$r = 0.1$	0.238749	0.282729	0.844444

mistuning causes the repeated eigenvalues of the unperturbed system to "split", and a few modes associated with these now simple eigenvalues become active.

5.2. Case 2

Fig. 5.4 shows the displacement solutions of the connected 16th and 32nd blocks for the unperturbed system and for typical realizations of the perturbed system with increasing mistuning parameter r. The displacements of the blocks exhibit a very different behavior from what we have seen by Case 1. These displacement solutions suggest that the two dominant frequencies are much closer to each other than those of Case 1, which causes beats in the displacement solution. Moreover the frequency of the beats is hardly affected by the mistuning of masses.

Indeed, the energy spectral density of $x_{32}(t)$ depicted in Fig. 5.5 shows that the two dominant frequencies are close to each other, while Table 5.2 also shows that their values remain practically unchanged despite the mistuning. These two eigenfrequencies happen to be the lowest ones. Hence, they are the least affected by the mistuning as discussed in Section 4, this is why the displacement solutions are less sensitive to the mistuning in this case.

6. Summary and discussion

We studied the mechanistic turbulence model (Fig. 1.1), a binary tree-structured MDoF linear oscillator described by the equation of motion (2.1). We chose a set of parameters defined by Eq. (2.5) for our study.

We proved a recursive formula for the characteristic polynomial of the undamped system described by Eq. (3.3), and derived an alternative formulation given in Eq. (3.10) as a product of generalized Chebyshev polynomials. This provided a more efficient way

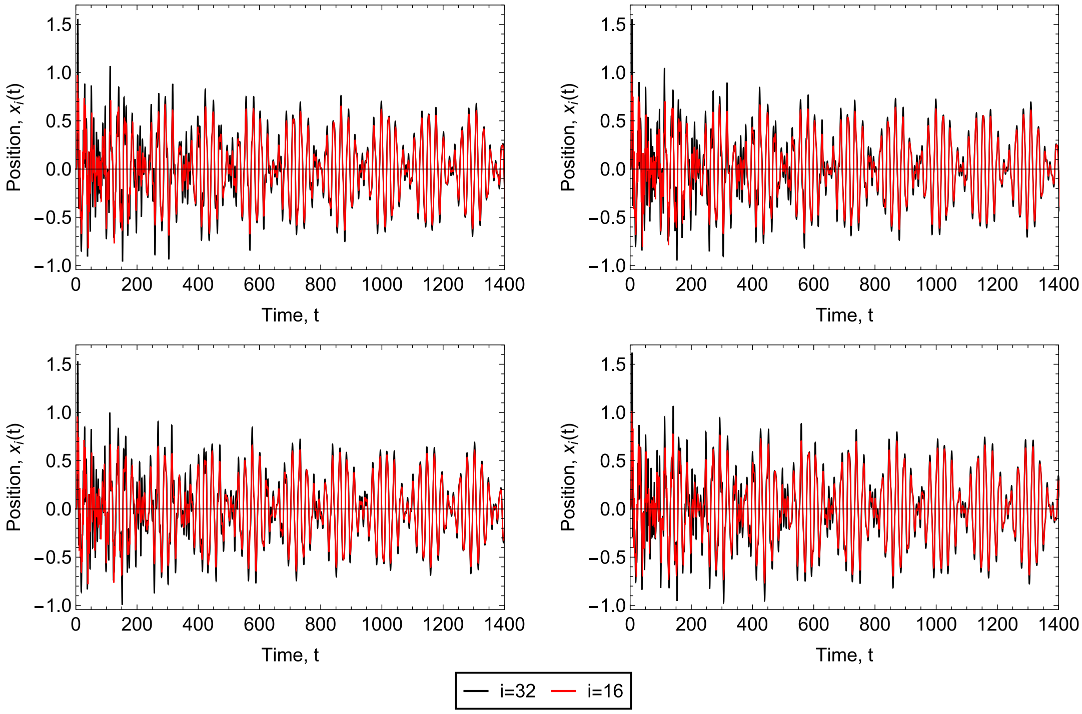

Fig. 5.4. Displacement solution of the 16th and 32nd blocks with Eq. (5.2) and (5.3) for the unperturbed system (top left), $r = 0.02$ (top right), $r = 0.05$ (bottom left), and $r = 0.1$ (bottom right).

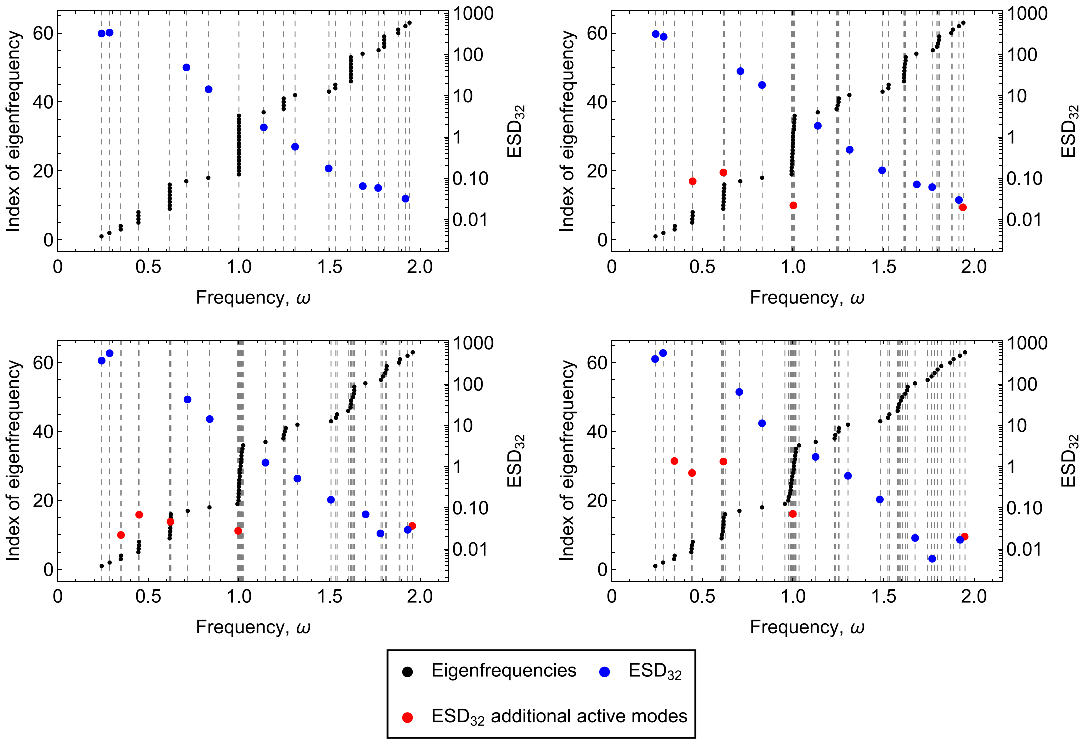

Fig. 5.5. Energy spectral density of $x_{32}(t)$ and the eigenvalue distribution of the system with initial conditions (5.2) and (5.3) for $r = 0$ (top left), $r = 0.02$ (top right), $r = 0.05$ (bottom left), and $r = 0.1$ (bottom right).

of calculating the eigenvalues of the system compared to directly solving the characteristic Eq. (3.5). The roots of the characteristic polynomial in Eq. (3.10) were derived for $\sigma = 1/2$, which are generated by the angles $\theta_{l,i}$ given in Eq. (3.22).

The eigenvalue distribution of the unperturbed system exhibits a self-similar structure which resembles the Devil's staircase function. Knowing the exact eigenvalues for $\sigma = 1/2$ enabled the derivation of a lower and an upper bound of the distribution function $F_n(z)$ given in Eq. (3.24). As demonstrated in Theorem 3, these bounds converge to the same $h(z)$ function given in Eq. (3.29), which is related to the Devil's staircase function $g(z)$ of Eq. (3.28) discussed in detail in [15].

We examined the effects of random mistuning of the block masses of the system according to Eq. (4.1). As a result of the mistuning process, the Devil's staircase falls apart, i.e., the repeated eigenvalues of the system break up into distinct eigenvalues. As the mistuning parameter r is increased, the larger eigenvalues are also perturbed to a greater extent than the smaller ones, extending the range covered by the eigenvalue distribution. To demonstrate the impact of the mistuning on the dynamics of the system, the equation of motion (2.1) was solved with two types of initial conditions for the unperturbed and perturbed systems for different values of the mistuning parameter r.

For the in-phase initial conditions defined by Eq. (5.1), the displacement solutions changed significantly by the mistuning process. While the main oscillation frequency remained practically the same, the envelope of the displacement solution was sensitive to the small changes of the eigenfrequencies. In contrast, the out-of-phase initial condition (5.2) resulted in beating. In this case the dominant active modes corresponded to the two smallest eigenfrequencies which were the least affected by the mistuning. As a result of this, the frequency of the beats showed resilience against the mistuning.

In the future, we plan to show analytically the sensitivity of the oscillation envelope on the particular eigenfrequencies of mistuned systems. We also plan to derive and prove a more general formula for the characteristic polynomial (3.6). For example, we are interested in deriving the characteristic polynomial for damped systems. We also intend to study m-ary tree-structured systems, i.e., when the oscillator has more than two branches emanating from each block.

CRediT authorship contribution statement

Róbert Rochlitz: Writing – review & editing, Writing – original draft, Visualization, Methodology, Investigation, Formal analysis. **Bendegúz Dezső Bak:** Writing – review & editing, Writing – original draft, Visualization, Supervision, Project administration, Methodology, Conceptualization. **Tamás Kalmár-Nagy:** Writing – review & editing, Writing – original draft, Supervision, Resources, Conceptualization.

Declaration of competing interest

The authors declare that they have no known competing financial interests or personal relationships that could have appeared to influence the work reported in this paper.

Acknowledgments

The research reported in this paper is part of project no. TKP-6-6/PALY-2021. Project no. TKP-6-6/PALY-2021 has been implemented with the support provided by the Ministry of Culture and Innovation of Hungary from the National Research, Development and Innovation Fund, financed under the TKP2021-NVA funding scheme.

This work has been supported by the Hungarian National Research, Development and Innovation Fund under contract NKFI K 137726.

One of the authors, Bendegúz Dezső Bak has also been supported by the János Bolyai Research Scholarship of the Hungarian Academy of Sciences.

Declaration of Generative AI and AI-assisted technologies in the writing process

The authors declare that they have not used any generative AI software tools in writing this paper.

Appendix A. Characteristic equation of the mechanistic turbulence model

Theorem 1. The characteristic polynomial of the system described by Eq. (3.3) has the form

$$\begin{aligned}\det(\mathbf{A}_n(\lambda)) &= \sigma^{2+(n-2)2^n} P_n(\lambda),\\ P_n(\lambda) &= \frac{Q_n(\lambda)}{Q_{n-1}(\lambda)} P_{n-1}^2(\lambda),\end{aligned} \tag{A.1}$$

where

$$\begin{aligned}P_0(\lambda) &= Q_0(\lambda) = 1,\\ Q_n(\lambda) &= q^n U_n\left(\frac{\lambda^2+a}{b}\right) - 2\sigma K_1 q^{n-1} U_{n-1}\left(\frac{\lambda^2+a}{b}\right),\\ a &= \frac{K_1}{M_1}(1+2\sigma), \quad b = \frac{2K_1}{M_1}\sqrt{2\sigma}, \quad q = K_1\sqrt{2\sigma},\end{aligned} \tag{A.2}$$

and U_n are Chebyshev polynomials of the second kind.

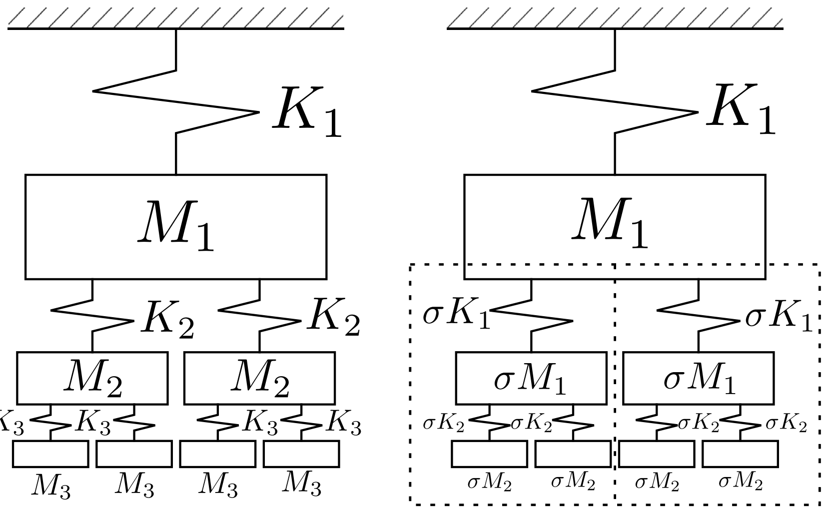

Fig. A.1. The undamped mechanistic turbulence model with $n = 3$ levels and ungrounded last level (left), and the scaling property of the model (right).

Proof. We prove Theorem 1. by induction. For $n = 1$, the characteristic polynomial is

$$\det(\mathbf{A}_1(\lambda)) = M_1\lambda^2 + K_1. \tag{A.3}$$

Using Eq. (A.1), we get

$$\begin{aligned}\det(\mathbf{A}_1(\lambda)) &= P_1(\lambda) = \frac{Q_1(\lambda)}{Q_0(\lambda)}P_0^2(\lambda) = Q_1(\lambda) = K_1\sqrt{2\sigma}U_1\left(\frac{\lambda^2+a}{b}\right) - 2\sigma K_1 \\ &= 2K_1\sqrt{2\sigma}\frac{\lambda^2+a}{b} - 2\sigma K_1 = \frac{2K_1\sqrt{2\sigma}}{\frac{2K_1}{M_1}\sqrt{2\sigma}}\lambda^2 + \frac{1+2\sigma}{2\sqrt{2\sigma}}2K_1\sqrt{2\sigma} - 2\sigma K_1 \\ &= M_1\lambda^2 + K_1.\end{aligned} \tag{A.4}$$

Now we assume that Eq. (A.1) holds up to some $n \geq 1$. The key idea of the proof is that the binary tree with $n \geq 2$ can be thought of as two binary trees with $n - 1$ levels and parameters scaled by σ being connected to the first block that has a mass of M_1, as shown in Fig. A.1. By rearranging the rows and columns of $\mathbf{A}_{n+1}(\lambda)$ accordingly, the characteristic polynomial takes the form

$$\det(\mathbf{A}_{n+1}(\lambda)) = \begin{vmatrix} \sigma\mathbf{A}_n(\lambda) & \mathbf{a}_n & \mathbf{0}_n \\ \mathbf{a}_n^{\mathrm{T}} & P_1(\lambda) + 2\sigma K_1 & \mathbf{a}_n^{\mathrm{T}} \\ \mathbf{0}_n & \mathbf{a}_n & \sigma\mathbf{A}_n(\lambda) \end{vmatrix} = \begin{vmatrix} \sigma\mathbf{A}_n(\lambda) & \mathbf{B}_n \\ \mathbf{B}_n^{\mathrm{T}} & \mathbf{D}_n(\lambda) \end{vmatrix}, \tag{A.5}$$

where

$$\begin{aligned}\mathbf{a}_n &= \begin{bmatrix} -\sigma K_1 \\ 0 \\ \vdots \\ 0 \end{bmatrix} \in \mathbb{R}^{(2^n-1)}, \\ \mathbf{0}_n &= \begin{bmatrix} 0 & \dots & 0 \\ \vdots & \ddots & \vdots \\ 0 & \dots & 0 \end{bmatrix} \in \mathbb{R}^{(2^n-1)\times(2^n-1)}, \\ \mathbf{B}_n &= \begin{bmatrix} \mathbf{a}_n & \mathbf{0}_n \end{bmatrix}, \\ \mathbf{D}_n(\lambda) &= \begin{bmatrix} P_1(\lambda) + 2\sigma K_1 & \mathbf{a}_n^{\mathrm{T}} \\ \mathbf{a}_n & \sigma\mathbf{A}_n(\lambda) \end{bmatrix}.\end{aligned} \tag{A.6}$$

Using the expression for the determinant of a 2×2 block matrix, we get

$$\begin{aligned}\det(\mathbf{A}_{n+1}(\lambda)) &= \det(\sigma\mathbf{A}_n(\lambda))\det(\mathbf{D}_n(\lambda) - \mathbf{B}_n^{\mathrm{T}}(\sigma\mathbf{A}_n(\lambda))^{-1}\mathbf{B}_n) \\ &= \sigma^{N(n)+2^n-1}P_n(\lambda)\det(\mathbf{D}_n(\lambda) - \sigma^{-1}\mathbf{B}_n^{\mathrm{T}}\mathbf{A}_n^{-1}(\lambda)\mathbf{B}_n),\end{aligned} \tag{A.7}$$

where

$$N(n) = 2 + (n-2)2^n. \tag{A.8}$$

As $\left[\mathbf{B}_n\right]_{i,j} = -\delta_{1,i}\delta_{1,j}\sigma K_1$, where δ denotes the Kronecker delta, the product $\mathbf{B}_n^{\mathrm{T}}\mathbf{A}_n^{-1}(\lambda)\mathbf{B}_n$ will have only one non-zero element, i.e.,

$$\left[\mathbf{B}_n^{\mathrm{T}}\mathbf{A}_n^{-1}(\lambda)\mathbf{B}_n\right]_{i,j} = \sum_{s,u=1}^{2^n-1}\left(\left[\mathbf{B}_n^{\mathrm{T}}\right]_{i,s}\left[\mathbf{A}_n^{-1}(\lambda)\right]_{s,u}\left[\mathbf{B}_n\right]_{u,j}\right) = \delta_{1,i}\delta_{1,j}\sigma^2 K_1^2\left[\mathbf{A}_n^{-1}(\lambda)\right]_{i,j}. \tag{A.9}$$

The (1,1)-th element of the inverse can be calculated using Cramer's rule, i.e.,

$$\left[\mathbf{A}_n^{-1}(\lambda)\right]_{1,1} = \frac{1}{\det(\mathbf{A}_n(\lambda))}A_{1,1}(\lambda), \tag{A.10}$$

where $A_{1,1}(\lambda)$ is the minor corresponding to the $(1,1)$-th element of $\mathbf{A}_n(\lambda)$. Once again, we use the scaling property of the binary tree to rearrange the rows and columns of the minor, thus we get

$$A_{1,1}(\lambda) = \begin{vmatrix}\sigma\mathbf{A}_{n-1}(\lambda) & \mathbf{0}_{n-1}\\ \mathbf{0}_{n-1} & \sigma\mathbf{A}_{n-1}(\lambda)\end{vmatrix} = \det(\sigma\mathbf{A}_{n-1}(\lambda))^2 = \sigma^{2N(n-1)+2^n-2}P_{n-1}^2(\lambda). \tag{A.11}$$

Substituting Eqs. (A.1) and (A.11) into Eq. (A.10) yields

$$\begin{aligned}\left[\mathbf{A}_n^{-1}(\lambda)\right]_{1,1} &= \sigma^{-N(n)+2N(n-1)+2^n-2}\frac{P_{n-1}^2(\lambda)}{P_n(\lambda)},\\ \left[\mathbf{B}_n^{\mathrm{T}}\mathbf{A}_n^{-1}(\lambda)\mathbf{B}_n\right]_{1,1} &= \sigma^{-N(n)+2N(n-1)+2^n}K_1^2\frac{P_{n-1}^2(\lambda)}{P_n(\lambda)},\end{aligned} \tag{A.12}$$

where the exponents of σ yield

$$\begin{aligned}-N(n)+2N(n-1)+2^n-2 &= -\left[(n-2)2^n+2\right]+2\left[(n-3)2^{n-1}+2\right]+2^n-2 = 0,\\ -N(n)+2N(n-1)+2^n &= -\left[(n-2)2^n+2\right]+2\left[(n-3)2^{n-1}+2\right]+2^n = 2.\end{aligned} \tag{A.13}$$

Substituting Eq. (A.12) into Eq. (A.7) yields

$$\begin{aligned}\det(\mathbf{A}_{n+1}(\lambda)) &= \sigma^{N(n)+2^n-1}P_n(\lambda)\begin{vmatrix}P_1(\lambda)+2\sigma K_1-\sigma K_1^2\frac{P_{n-1}^2(\lambda)}{P_n(\lambda)} & \mathbf{a}_n^{\mathrm{T}}\\ \mathbf{a}_n & \sigma\mathbf{A}_n(\lambda)\end{vmatrix}\\ &= \sigma^{N(n)+2^n-1}P_n(\lambda)\det(\sigma\mathbf{A}_n(\lambda))\\ &\quad\cdot\left[\left(P_1(\lambda)+2\sigma K_1-\sigma K_1^2\frac{P_{n-1}^2(\lambda)}{P_n(\lambda)}\right)-\sigma^{-1}\mathbf{a}_n^{\mathrm{T}}\mathbf{A}_n^{-1}(\lambda)\mathbf{a}_n\right].\end{aligned} \tag{A.14}$$

As $[\mathbf{a}_n]_{i,1} = -\delta_{1,i}\sigma K_1$, we have

$$\begin{aligned}\mathbf{a}_n^{\mathrm{T}}\mathbf{A}_n^{-1}(\lambda)\mathbf{a}_n &= \sum_{s,u=1}^{2^n-1}\left(\left[\mathbf{a}_n^{\mathrm{T}}\right]_{1,s}\left[\mathbf{A}_n^{-1}(\lambda)\right]_{s,u}[\mathbf{a}_n]_{u,1}\right) = \left[\mathbf{a}_n^{\mathrm{T}}\right]_{1,1}\left[\mathbf{A}_n^{-1}(\lambda)\right]_{1,1}[\mathbf{a}_n]_{1,1}\\ &= \sigma^2K_1^2\left[\mathbf{A}_n^{-1}(\lambda)\right]_{1,1} = \sigma^2K_1^2\frac{P_{n-1}^2(\lambda)}{P_n(\lambda)}.\end{aligned} \tag{A.15}$$

Substituting into Eq. (A.14) leads to

$$\det(\mathbf{A}_{n+1}(\lambda)) = \sigma^{2\left[N(n)+2^n-1\right]}P_n^2(\lambda)\left(P_1(\lambda)+2\sigma K_1-2\sigma K_1^2\frac{P_{n-1}^2(\lambda)}{P_n(\lambda)}\right). \tag{A.16}$$

For the exponent of σ we get

$$\begin{aligned}&2\left[N(n)+2^n-1\right] = 2N(n)+2^{n+1}-2 = 2\left[(n-2)2^n+2\right]+2^{n+1}-2\\ &= (n-2)2^{n+1}+4+2^{n+1}-2 = (n-1)2^{n+1}+2 = N(n+1).\end{aligned} \tag{A.17}$$

Based on Eq. (A.1) we have

$$\frac{P_{n-1}^2(\lambda)}{P_n(\lambda)} = \frac{Q_{n-1}(\lambda)}{Q_n(\lambda)}, \tag{A.18}$$

thus

$$\det(\mathbf{A}_{n+1}(\lambda)) = \sigma^{N(n+1)}P_n^2(\lambda)\frac{(P_1(\lambda)+2\sigma)Q_n(\lambda)-2\sigma K_1^2Q_{n-1}(\lambda)}{Q_n(\lambda)}. \tag{A.19}$$

All that is left to show is that

$$Q_{n+1}(\lambda) = (P_1(\lambda) + 2\sigma K_1)Q_n(\lambda) - 2\sigma K_1^2 Q_{n-1}(\lambda). \tag{A.20}$$

Using the fact that $U_n(x) = 2xU_{n-1}(x) - U_{n-2}(x)$ and $U_1(x) = 2x$, Q_{n+1} for $n \geq 2$ can be written as

$$\begin{aligned}
Q_{n+1}(\lambda) &= \left(K_1\sqrt{2\sigma}\right)^{n+1} U_{n+1}\left(\frac{\lambda^2+a}{b}\right) - 2\sigma K_1 \left(K_1\sqrt{2\sigma}\right)^{n} U_{n}\left(\frac{\lambda^2+a}{b}\right) \\
&= \left(K_1\sqrt{2\sigma}\right)^{n+1}\left[2\frac{\lambda^2+a}{b}U_n\left(\frac{\lambda^2+a}{b}\right) - U_{n-1}\left(\frac{\lambda^2+a}{b}\right)\right] \\
&\quad - 2\sigma K_1\left(K_1\sqrt{2\sigma}\right)^{n}\left[2\frac{\lambda^2+a}{b}U_{n-1}\left(\frac{\lambda^2+a}{b}\right) - U_{n-2}\left(\frac{\lambda^2+a}{b}\right)\right] \\
&= 2k_1\sqrt{2\sigma}\frac{\lambda^2+a}{b}\left[\left(K_1\sqrt{2\sigma}\right)^{n}U_n\left(\frac{\lambda^2+a}{b}\right) - 2\sigma K_1\left(K_1\sqrt{2\sigma}\right)^{n-1}U_{n-1}\left(\frac{\lambda^2+a}{b}\right)\right] \\
&\quad - \left(K_1\sqrt{2\sigma}\right)^{2}\left[\left(K_1\sqrt{2\sigma}\right)^{n-1}U_{n-1}\left(\frac{\lambda^2+a}{b}\right) - 2\sigma K_1\left(K_1\sqrt{2\sigma}\right)^{n-2}U_{n-2}\left(\frac{\lambda^2+a}{b}\right)\right] \\
&= \left[K_1\sqrt{2\sigma}U_1\left(\frac{\lambda^2+a}{b}\right) - 2\sigma K_1 + 2\sigma K_1\right]Q_n(\lambda) - 2\sigma K_1^2 Q_{n-1}(\lambda) \\
&= \left(P_1(\lambda) + 2\sigma K_1\right)Q_n(\lambda) - 2\sigma K_1^2 Q_{n-1}(\lambda).
\end{aligned} \tag{A.21}$$

As U_{-1} is not defined, the case of $n = 1$ must be handled separately as

$$\begin{aligned}
Q_2(\lambda) &= \left(K_1\sqrt{2\sigma}\right)^{2} U_2\left(\frac{\lambda^2+a}{b}\right) - 2\sigma K_1\left(K_1\sqrt{2\sigma}\right)U_1\left(\frac{\lambda^2+a}{b}\right) \\
&= \left(K_1\sqrt{2\sigma}\right)^{2}\left[2\frac{\lambda^2+a}{b}U_1\left(\frac{\lambda^2+a}{b}\right) - U_0\left(\frac{\lambda^2+a}{b}\right)\right] - 2\sigma K_1\left(K_1\sqrt{2\sigma}\right)U_1\left(\frac{\lambda^2+a}{b}\right) \\
&= K_1\sqrt{2\sigma}\left[K_1\sqrt{2\sigma}U_1\left(\frac{\lambda^2+a}{b}\right) - 2\sigma K_1\right]U_1\left(\frac{\lambda^2+a}{b}\right) - 2\sigma K_1^2 \\
&= \left(P_1(\lambda) + 2\sigma K_1\right)Q_1(\lambda) - 2\sigma K_1^2 Q_0(\lambda).
\end{aligned} \qquad \square \tag{A.22}$$

Appendix B. Eigenvalue distribution of the mechanistic turbulence model

Theorem 2. For any $n \geq 2$, $z \in [0, \sqrt{a+b}]$ pair, the function $h_n(z)$ defined by Eq. (3.25), and the distribution function $F_n(z)$ given by Eq. (3.24) corresponding to the characteristic polynomial $P_n(\lambda) = \det(\lambda^2\mathbf{M}_n + \mathbf{K}_n)$ of system (3.3) with $\sigma = 1/2$ satisfy the relationship

$$h_n\left(\frac{1}{\pi}\arccos\left(\frac{a-z^2}{b}\right)\right) \leq F_n(z) \leq h_n\left(\frac{1}{\pi}\arccos\left(\frac{a-z^2}{b}\right)\right) + \frac{n}{2^n}. \tag{B.1}$$

Proof. By substituting $\frac{1}{\pi}\arccos\left(\frac{a-z^2}{b}\right)$ into the argument of $h_n(z)$, we can conclude that for any $z \in [0, \sqrt{a+b}]$ Eq. (3.25) becomes

$$h_n\left(\frac{1}{\pi}\arccos\left(\frac{a-z^2}{b}\right)\right) = \frac{\#\left\{\lambda : \frac{\det(\lambda^2\mathbf{M}_n+\mathbf{K}_n)}{Q_n(\lambda)} = 0,\ 0 < \mathrm{Im}(\lambda) \leq z\right\}}{2^n}. \tag{B.2}$$

Since $Q_n(\lambda)$ is a factor of $\det(\lambda^2\mathbf{M}_n + \mathbf{K}_n)$ according to Corollary 2., the expression

$$\frac{\det(\lambda^2\mathbf{M}_n + \mathbf{K}_n)}{Q_n(\lambda)} = 0 \tag{B.3}$$

must have fewer roots than $\det(\lambda^2\mathbf{M}_n + \mathbf{K}_n) = 0$, therefore, the lower bound of $F_n(z)$ is expressed as

$$h_n\left(\frac{1}{\pi}\arccos\left(\frac{a-z^2}{b}\right)\right) \leq F_n(z). \tag{B.4}$$

$Q_n(\lambda)$, as defined in Eq. (3.6), has $2n$ solutions, thus

$$\#\left\{\lambda : Q_n(\lambda) = 0,\ 0 < \mathrm{Im}(\lambda)\right\} = n. \tag{B.5}$$

The upper bound of $F_n(z)$ is derived as

$$\begin{aligned}
&\#\left\{\lambda : \det(\lambda^2\mathbf{M}_n+\mathbf{K}_n)=0,\ 0<\mathrm{Im}(\lambda)\le z\right\}\\
&=\left(\#\left\{\lambda : \frac{\det(\lambda^2\mathbf{M}_n+\mathbf{K}_n)}{Q_n(\lambda)}=0,\ 0<\mathrm{Im}(\lambda)\le z\right\}\right)\\
&\quad+\left(\#\left\{\lambda : Q_n(\lambda)=0,\ 0<\mathrm{Im}(\lambda)\le z\right\}\right)\\
&\le\left(\#\left\{\lambda : \frac{\det(\lambda^2\mathbf{M}_n+\mathbf{K}_n)}{Q_n(\lambda)}=0,\ 0<\mathrm{Im}(\lambda)\le z\right\}\right)+\left(\#\left\{\lambda : Q_n(\lambda)=0,\ 0<\mathrm{Im}(\lambda)\right\}\right)\\
&=\#\left\{\lambda : \frac{\det(\lambda^2\mathbf{M}_n+\mathbf{K}_n)}{Q_n(\lambda)}=0,\ 0<\mathrm{Im}(\lambda)\le z\right\}+n.
\end{aligned} \tag{B.6}$$

Thus, we have the upper bound

$$F_n(z)\le h_n\left(\frac{1}{\pi}\arccos\left(\frac{a-z^2}{b}\right)\right)+\frac{n}{2^n}.\quad\square \tag{B.7}$$

Theorem 3. The distribution function $F_n(z)$ given by Eq. (3.24) corresponding to the characteristic polynomial $P_n(\lambda)=\det(\lambda^2\mathbf{M}_n+\mathbf{K}_n)$ of system (3.3) with $\sigma=1/2$ satisfies the relationship

$$F(z)=\lim_{n\to\infty}F_n(z)=h\left(\frac{1}{\pi}\arccos\left(\frac{a-z^2}{b}\right)\right), \tag{B.8}$$

where $z\in[0,\sqrt{a+b})$, and $h(z)$ is defined in Eq. (3.29).

Proof. Since

$$\lim_{n\to\infty}\frac{n}{2^n}=0, \tag{B.9}$$

applying the squeeze theorem to Theorem 2 implies

$$F(z)=\lim_{n\to\infty}h_n\left(\frac{1}{\pi}\arccos\left(\frac{a-z^2}{b}\right)\right),\qquad z\in[0,\sqrt{a+b}). \tag{B.10}$$

Next, we seek an alternative representation of $h_n(z)$ which enables us to determine its limit in $n\to\infty$. Eq. (3.22) implies that for $z\in[0,1)$,

$$0<\mathrm{Im}(\lambda)\le\sqrt{a-b\cos(z\pi)}\iff\frac{2j-1}{2l-1}\le z,\quad 1\le j\le l-1,\ 1\le l\le n. \tag{B.11}$$

Then, for every $0\le z<1$ and $n\ge 2$ pair, we define

$$\mathcal{A}_n(z)=\left\{(j,l) : \frac{2j-1}{2l-1}\le z,\ 1\le j\le l-1,\ 1\le l\le n\right\}. \tag{B.12}$$

Using Corollary 2, we can factorize the polynomial in the definition of $h_n(z)$ as

$$\frac{\det(\lambda^2\mathbf{M}_n+\mathbf{K}_n)}{Q_n(\lambda)}=\prod_{l=0}^{n-1}Q_{n-1-l}^{2^l}(\lambda)=\prod_{l=1}^{n}Q_{l-1}^{2^{n-l}}(\lambda)=\prod_{l=2}^{n}Q_{l-1}^{2^{n-l}}(\lambda). \tag{B.13}$$

With the multiplicity of the $Q_l(\lambda)$ factors known, $h_n(z)$ can alternatively be written as

$$h_n(z)=\sum_{(j,l)\in\mathcal{A}_n(z)}\frac{2^{n-l}}{2^n}=\sum_{(j,l)\in\mathcal{A}_n(z)}\frac{1}{2^l},\quad 0\le z<1. \tag{B.14}$$

Let

$$\mathcal{B}_l(z)=\{(j,l) : 2j-1\le(2l-1)z\},\quad l\in\mathbb{Z}, \tag{B.15}$$

then

$$\mathcal{A}_n(z)=\bigcup_{l=1}^{n}\mathcal{B}_l(z). \tag{B.16}$$

Substituting this into Eq. (B.14) yields

$$h_n(z)=\sum_{l=1}^{n}\sum_{(j,l)\in\mathcal{B}_l(z)}\frac{1}{2^l}=\sum_{l=1}^{n}\frac{1}{2^l}\left\lfloor\frac{(2l-1)z+1}{2}\right\rfloor,\quad 0\le z<1. \tag{B.17}$$

Clearly,

$$\lim_{n\to\infty}h_n(z)=h(z),\quad 0\le z<1, \tag{B.18}$$

thus for any $z \in [0, \sqrt{a+b})$,

$$F(z) = \lim_{n\to\infty} h_n\left(\frac{1}{\pi}\arccos\left(\frac{a-z^2}{b}\right)\right) = h\left(\frac{1}{\pi}\arccos\left(\frac{a-z^2}{b}\right)\right). \quad \square \tag{B.19}$$

Appendix C. Characteristic equation of the grounded mechanistic turbulence model

Theorem 4. The characteristic polynomial of the system described by Eq. (3.32) has the form

$$\begin{aligned} \det(\mathbf{A}_n(\lambda)) &= \sigma^{2+(n-2)2^n} P_n(\lambda), \\ P_n(\lambda) &= \frac{Q_n(\lambda)}{Q_{n-1}(\lambda)} P_{n-1}^2(\lambda), \end{aligned} \tag{C.1}$$

where

$$P_0(\lambda) = Q_0(\lambda) = 1,$$

$$Q_n(\lambda) = q^n U_n\left(\frac{\lambda^2+a}{b}\right) - \sigma K_1 q^{n-1} U_{n-1}\left(\frac{\lambda^2+a}{b}\right),$$

$$a = \frac{K_1}{M_1}(1+2\sigma), \quad b = \frac{2K_1}{M_1}\sqrt{2\sigma}, \quad q = K_1\sqrt{2\sigma},$$

and U_n are Chebyshev polynomials of the second kind.

Proof. We prove Theorem 4. by induction. For $n=1$, the characteristic polynomial is

$$\det(\mathbf{A}_1(\lambda)) = M_1\lambda^2 + K_1(1+\sigma). \tag{C.2}$$

Using Eq. (C.1), we get

$$\begin{aligned} \det(\mathbf{A}_1(\lambda)) = P_1(\lambda) &= \frac{Q_1(\lambda)}{Q_0(\lambda)} P_0^2(\lambda) = Q_1(\lambda) = K_1\sqrt{2\sigma} U_1\left(\frac{\lambda^2+a}{b}\right) - \sigma K_1 \\ &= 2K_1\sqrt{2\sigma}\frac{\lambda^2+a}{b} - \sigma K_1 = \frac{2K_1\sqrt{2\sigma}}{\frac{2K_1}{M_1}\sqrt{2\sigma}}\lambda^2 + \frac{1+2\sigma}{2\sqrt{2\sigma}} 2K_1\sqrt{2\sigma} - \sigma K_1 \\ &= M_1\lambda^2 + K_1(1+\sigma). \end{aligned} \tag{C.3}$$

Now we assume that Eq. (C.1) holds up to some $n \ge 1$. The key idea of the proof is that the binary tree with $n \ge 2$ can be thought of as two binary trees with $n-1$ levels and parameters scaled by σ being connected to the first block that has a mass of M_1, as shown in Fig. A.1. By rearranging the rows and columns of $\mathbf{A}_{n+1}(\lambda)$ accordingly, the characteristic polynomial takes the form

$$\det(\mathbf{A}_{n+1}(\lambda)) = \begin{vmatrix} \sigma\mathbf{A}_n(\lambda) & \mathbf{a}_n & \mathbf{0}_n \\ \mathbf{a}_n^{\mathrm{T}} & P_1(\lambda)+\sigma K_1 & \mathbf{a}_n^{\mathrm{T}} \\ \mathbf{0}_n & \mathbf{a}_n & \sigma\mathbf{A}_n(\lambda) \end{vmatrix} = \begin{vmatrix} \sigma\mathbf{A}_n(\lambda) & \mathbf{B}_n \\ \mathbf{B}_n^{\mathrm{T}} & \mathbf{D}_n(\lambda) \end{vmatrix}, \tag{C.4}$$

where

$$\begin{aligned} \mathbf{a}_n &= \begin{bmatrix} -\sigma K_1 \\ 0 \\ \vdots \\ 0 \end{bmatrix} \in \mathbb{R}^{(2^n-1)}, \\ \mathbf{0}_n &= \begin{bmatrix} 0 & \dots & 0 \\ \vdots & \ddots & \vdots \\ 0 & \dots & 0 \end{bmatrix} \in \mathbb{R}^{(2^n-1)\times(2^n-1)}, \\ \mathbf{B}_n &= \begin{bmatrix} \mathbf{a}_n & \mathbf{0}_n \end{bmatrix}, \\ \mathbf{D}_n(\lambda) &= \begin{bmatrix} P_1(\lambda)+\sigma K_1 & \mathbf{a}_n^{\mathrm{T}} \\ \mathbf{a}_n & \sigma\mathbf{A}_n(\lambda) \end{bmatrix}. \end{aligned} \tag{C.5}$$

Using the expression for the determinant of a 2×2 block matrix, we get

$$\begin{aligned} \det(\mathbf{A}_{n+1}(\lambda)) &= \det(\sigma\mathbf{A}_n(\lambda))\det(\mathbf{D}_n(\lambda) - \mathbf{B}_n^{\mathrm{T}}(\sigma\mathbf{A}_n(\lambda))^{-1}\mathbf{B}_n) \\ &= \sigma^{N(n)+2^n-1} P_n(\lambda)\det(\mathbf{D}_n(\lambda) - \sigma^{-1}\mathbf{B}_n^{\mathrm{T}}\mathbf{A}_n^{-1}(\lambda)\mathbf{B}_n), \end{aligned} \tag{C.6}$$

where

$$N(n) = 2 + (n-2)2^n. \tag{C.7}$$

As $\left[\mathbf{B}_n\right]_{i,j} = -\delta_{1,i}\delta_{1,j}\sigma K_1$, where δ denotes the Kronecker delta, the product $\mathbf{B}_n^{\mathrm{T}}\mathbf{A}_n^{-1}(\lambda)\mathbf{B}_n$ will have only one non-zero element, i.e.,

$$\left[\mathbf{B}_n^{\mathrm{T}}\mathbf{A}_n^{-1}(\lambda)\mathbf{B}_n\right]_{i,j} = \sum_{s,u=1}^{2^n-1}\left(\left[\mathbf{B}_n^{\mathrm{T}}\right]_{i,s}\left[\mathbf{A}_n^{-1}(\lambda)\right]_{s,u}\left[\mathbf{B}_n\right]_{u,j}\right) = \delta_{1,i}\delta_{1,j}\sigma^2 K_1^2\left[\mathbf{A}_n^{-1}(\lambda)\right]_{i,j}. \tag{C.8}$$

The (1,1)-th element of the inverse can be calculated using Cramer's rule, i.e.,

$$\left[\mathbf{A}_n^{-1}(\lambda)\right]_{1,1} = \frac{1}{\det(\mathbf{A}_n(\lambda))}A_{1,1}(\lambda), \tag{C.9}$$

where $A_{1,1}(\lambda)$ is the minor corresponding to the $(1,1)$-th element of $\mathbf{A}_n(\lambda)$. Once again, we use the scaling property of the binary tree to rearrange the rows and columns of the minor, thus we get

$$A_{1,1}(\lambda) = \begin{vmatrix}\sigma\mathbf{A}_{n-1}(\lambda) & \mathbf{0}_{n-1}\\ \mathbf{0}_{n-1} & \sigma\mathbf{A}_{n-1}(\lambda)\end{vmatrix} = \det(\sigma\mathbf{A}_{n-1}(\lambda))^2 = \sigma^{2N(n-1)+2^n-2}P_{n-1}^2(\lambda). \tag{C.10}$$

Substituting Eqs. (C.1) and (C.10) into Eq. (C.9) yields

$$\begin{aligned}\left[\mathbf{A}_n^{-1}(\lambda)\right]_{1,1} &= \sigma^{-N(n)+2N(n-1)+2^n-2}\frac{P_{n-1}^2(\lambda)}{P_n(\lambda)},\\ \left[\mathbf{B}_n^{\mathrm{T}}\mathbf{A}_n^{-1}(\lambda)\mathbf{B}_n\right]_{1,1} &= \sigma^{-N(n)+2N(n-1)+2^n}K_1^2\frac{P_{n-1}^2(\lambda)}{P_n(\lambda)},\end{aligned} \tag{C.11}$$

where the exponents of σ yield

$$\begin{aligned}-N(n)+2N(n-1)+2^n-2 &= -\left[(n-2)2^n+2\right]+2\left[(n-3)2^{n-1}+2\right]+2^n-2 = 0,\\ -N(n)+2N(n-1)+2^n &= -\left[(n-2)2^n+2\right]+2\left[(n-3)2^{n-1}+2\right]+2^n = 2.\end{aligned} \tag{C.12}$$

Substituting Eq. (C.11) into Eq. (C.6) yields

$$\begin{aligned}\det(\mathbf{A}_{n+1}(\lambda)) &= \sigma^{N(n)+2^n-1}P_n(\lambda)\begin{vmatrix}P_1(\lambda)+\sigma K_1-\sigma K_1^2\frac{P_{n-1}^2(\lambda)}{P_n(\lambda)} & \mathbf{a}_n^{\mathrm{T}}\\ \mathbf{a}_n & \sigma\mathbf{A}_n(\lambda)\end{vmatrix}\\ &= \sigma^{N(n)+2^n-1}P_n(\lambda)\det(\sigma\mathbf{A}_n(\lambda))\\ &\quad\cdot\left[\left(P_1(\lambda)+\sigma K_1-\sigma K_1^2\frac{P_{n-1}^2(\lambda)}{P_n(\lambda)}\right)-\sigma^{-1}\mathbf{a}_n^{\mathrm{T}}\mathbf{A}_n^{-1}(\lambda)\mathbf{a}_n\right].\end{aligned} \tag{C.13}$$

As $[\mathbf{a}_n]_{i,1} = -\delta_{1,i}\sigma K_1$, we have

$$\begin{aligned}\mathbf{a}_n^{\mathrm{T}}\mathbf{A}_n^{-1}(\lambda)\mathbf{a}_n &= \sum_{s,u=1}^{2^n-1}\left(\left[\mathbf{a}_n^{\mathrm{T}}\right]_{1,s}\left[\mathbf{A}_n^{-1}(\lambda)\right]_{s,u}[\mathbf{a}_n]_{u,1}\right) = \left[\mathbf{a}_n^{\mathrm{T}}\right]_{1,1}\left[\mathbf{A}_n^{-1}(\lambda)\right]_{1,1}[\mathbf{a}_n]_{1,1}\\ &= \sigma^2K_1^2\left[\mathbf{A}_n^{-1}(\lambda)\right]_{1,1} = \sigma^2K_1^2\frac{P_{n-1}^2(\lambda)}{P_n(\lambda)}.\end{aligned} \tag{C.14}$$

Substituting into Eq. (C.13) leads to

$$\det(\mathbf{A}_{n+1}(\lambda)) = \sigma^{2\left[N(n)+2^n-1\right]}P_n^2(\lambda)\left(P_1(\lambda)+\sigma K_1-2\sigma K_1^2\frac{P_{n-1}^2(\lambda)}{P_n(\lambda)}\right). \tag{C.15}$$

For the exponent of σ we get

$$\begin{aligned}&2\left[N(n)+2^n-1\right] = 2N(n)+2^{n+1}-2 = 2\left[(n-2)2^n+2\right]+2^{n+1}-2\\ &= (n-2)2^{n+1}+4+2^{n+1}-2 = (n-1)2^{n+1}+2 = N(n+1).\end{aligned} \tag{C.16}$$

Based on Eq. (C.1) we have

$$\frac{P_{n-1}^2(\lambda)}{P_n(\lambda)} = \frac{Q_{n-1}(\lambda)}{Q_n(\lambda)}, \tag{C.17}$$

thus

$$\det(\mathbf{A}_{n+1}(\lambda)) = \sigma^{N(n+1)}P_n^2(\lambda)\frac{(P_1(\lambda)+\sigma)Q_n(\lambda)-2\sigma K_1^2Q_{n-1}(\lambda)}{Q_n(\lambda)}. \tag{C.18}$$

All that is left to show is that

$$Q_{n+1}(\lambda) = (P_1(\lambda) + \sigma K_1)Q_n(\lambda) - 2\sigma K_1^2 Q_{n-1}(\lambda). \tag{C.19}$$

Using the fact that $U_n(x) = 2xU_{n-1}(x) - U_{n-2}(x)$ and $U_1(x) = 2x$, Q_{n+1} for $n \geq 2$ can be written as

$$\begin{aligned}
Q_{n+1}(\lambda) &= \left(K_1\sqrt{2\sigma}\right)^{n+1} U_{n+1}\left(\frac{\lambda^2+a}{b}\right) - \sigma K_1 \left(K_1\sqrt{2\sigma}\right)^{n} U_{n}\left(\frac{\lambda^2+a}{b}\right) \\
&= \left(K_1\sqrt{2\sigma}\right)^{n+1}\left[2\frac{\lambda^2+a}{b}U_n\left(\frac{\lambda^2+a}{b}\right) - U_{n-1}\left(\frac{\lambda^2+a}{b}\right)\right] \\
&\quad - \sigma K_1\left(K_1\sqrt{2\sigma}\right)^{n}\left[2\frac{\lambda^2+a}{b}U_{n-1}\left(\frac{\lambda^2+a}{b}\right) - U_{n-2}\left(\frac{\lambda^2+a}{b}\right)\right] \\
&= 2k_1\sqrt{2\sigma}\frac{\lambda^2+a}{b}\left[\left(K_1\sqrt{2\sigma}\right)^{n}U_n\left(\frac{\lambda^2+a}{b}\right) - \sigma K_1\left(K_1\sqrt{2\sigma}\right)^{n-1}U_{n-1}\left(\frac{\lambda^2+a}{b}\right)\right] \\
&\quad - \left(K_1\sqrt{2\sigma}\right)^{2}\left[\left(K_1\sqrt{2\sigma}\right)^{n-1}U_{n-1}\left(\frac{\lambda^2+a}{b}\right) - \sigma K_1\left(K_1\sqrt{2\sigma}\right)^{n-2}U_{n-2}\left(\frac{\lambda^2+a}{b}\right)\right] \\
&= \left[K_1\sqrt{2\sigma}U_1\left(\frac{\lambda^2+a}{b}\right) - \sigma K_1 + \sigma K_1\right]Q_n(\lambda) - 2\sigma K_1^2 Q_{n-1}(\lambda) \\
&= \left(P_1(\lambda) + \sigma K_1\right)Q_n(\lambda) - 2\sigma K_1^2 Q_{n-1}(\lambda).
\end{aligned} \tag{C.20}$$

As U_{-1} is not defined, the case of $n = 1$ must be handled separately as

$$\begin{aligned}
Q_2(\lambda) &= \left(K_1\sqrt{2\sigma}\right)^{2}U_2\left(\frac{\lambda^2+a}{b}\right) - \sigma K_1\left(K_1\sqrt{2\sigma}\right)U_1\left(\frac{\lambda^2+a}{b}\right) \\
&= \left(K_1\sqrt{2\sigma}\right)^{2}\left[2\frac{\lambda^2+a}{b}U_1\left(\frac{\lambda^2+a}{b}\right) - U_0\left(\frac{\lambda^2+a}{b}\right)\right] - \sigma K_1\left(K_1\sqrt{2\sigma}\right)U_1\left(\frac{\lambda^2+a}{b}\right) \\
&= K_1\sqrt{2\sigma}\left[K_1\sqrt{2\sigma}U_1\left(\frac{\lambda^2+a}{b}\right) - \sigma K_1\right]U_1\left(\frac{\lambda^2+a}{b}\right) - 2\sigma K_1^2 \\
&= \left(P_1(\lambda) + \sigma K_1\right)Q_1(\lambda) - 2\sigma K_1^2 Q_0(\lambda). \quad \square
\end{aligned} \tag{C.21}$$

Data availability

Data will be made available on request.

References

[1] V.I. Arnold, Mathematical Methods of Classical Mechanics, vol. 60, Springer Science & Business Media, 2013.
[2] T. Kalmár-Nagy, B.D. Bak, An intriguing analogy of Kolmogorov's scaling law in a hierarchical mass–spring–damper model, Nonlinear Dynam. 95 (4) (2019) 3193–3203.
[3] H. Frahm, Device for damping vibrations of bodies, 1911, US Patent 989, 958.
[4] J.P. Den Hartog, Mechanical Vibration, McGraw-Hill, 1947.
[5] A.F. Vakakis, O.V. Gendelman, L.A. Bergman, D.M. McFarland, G. Kerschen, Y.S. Lee, Nonlinear Targeted Energy Transfer in Mechanical and Structural Systems, vol. 156, Springer Science & Business Media, 2008.
[6] H. Ding, L.Q. Chen, Designs, analysis, and applications of nonlinear energy sinks, Nonlinear Dynam. 100 (4) (2020) 3061–3107.
[7] M.A. Al-Shudeifat, A.S. Saeed, Frequency–energy plot and targeted energy transfer analysis of coupled bistable nonlinear energy sink with linear oscillator, Nonlinear Dynam. 105 (4) (2021) 2877–2898.
[8] Y.C. Zeng, H. Ding, R.H. Du, L.Q. Chen, Micro-amplitude vibration suppression of a bistable nonlinear energy sink constructed by a buckling beam, Nonlinear Dynam. 108 (4) (2022) 3185–3207.
[9] T. Wang, Q. Ding, Targeted energy transfer analysis of a nonlinear oscillator coupled with bistable nonlinear energy sink based on nonlinear normal modes, J. Sound Vib. 556 (2023) 117727.
[10] H. Li, A. Li, X. Kong, H. Xiong, Dynamics of an electromagnetic vibro-impact nonlinear energy sink, applications in energy harvesting and vibration absorption, Nonlinear Dynam. 108 (2) (2022) 1027–1043.
[11] Z. Wu, M. Paredes, S. Seguy, Targeted energy transfer in a vibro-impact cubic NES: Description of regimes and optimal design, J. Sound Vib. 545 (2023) 117425.
[12] R. Liu, R. Kuske, D. Yurchenko, Maps unlock the full dynamics of targeted energy transfer via a vibro-impact nonlinear energy sink, Mech. Syst. Signal Process. 191 (2023) 110158.

[13] T. Kalmár-Nagy, M. Kiss, Complexity in linear systems: a chaotic linear operator on the space of odd-periodic functions, Complexity 2017 (2017) Article ID 6020213, 8 pages.
[14] K. Kowalski, W.H. Steeb, Nonlinear Dynamical Systems and Carleman Linearization, World Scientific, 1991.
[15] T. Kalmár-Nagy, A. Amann, D. Kim, D. Rachinskii, The devil is in the details: spectrum and eigenvalue distribution of the discrete Preisach memory model, Commun. Nonlinear Sci. Numer. Simul. 77 (2019) 1–17.
[16] C. Song, S. Havlin, H.A. Makse, Self-similarity of complex networks, Nature 433 (7024) (2005) 392–395.
[17] L.F. Richardson, Weather Prediction by Numerical Process, Cambridge University Press, 1922.
[18] A.N. Kolmogorov, The local structure of turbulence in incompressible viscous fluid for very large Reynolds numbers, Dokl. Akad. Nauk SSSR 30 (4) (1941) 301–305.
[19] S.B. Pope, Turbulent Flows, Cambridge University Press, 2000.
[20] D.H. Zanette, Energy exchange between coupled mechanical oscillators: linear regimes, J. Phys. Commun. 2 (9) (2018) 095015.
[21] A.F. Vakakis, O.V. Gendelman, L.A. Bergman, A. Mojahed, M. Gzal, Nonlinear targeted energy transfer: state of the art and new perspectives, Nonlinear Dynam. 108 (2) (2022) 711–741.
[22] J.E. Chen, T. Theurich, M. Krack, T. Sapsis, L.A. Bergman, A.F. Vakakis, Intense cross-scale energy cascades resembling “mechanical turbulence” in harmonically driven strongly nonlinear hierarchical chains of oscillators, Acta Mech. 233 (4) (2022) 1289–1305.
[23] A.F. Vakakis, Inducing intentional strong nonlinearity in acoustics, in: Exploiting the Use of Strong Nonlinearity in Dynamics and Acoustics, Springer, 2024, pp. 1–47.
[24] B.D. Bak, R. Rochlitz, T. Kalmár-Nagy, Energy transfer mechanisms in binary tree-structured oscillator with nonlinear energy sinks, Nonlinear Dynam. 111 (11) (2023) 9875–9888.
[25] X. Huang, Y. Liu, Spectral structure and gap-labeling properties for a new class of one-dimensional quasilattices, Chin. Phys. Lett. 9 (11) (1992) 609.
[26] X. Fu, Y. Liu, P. Zhou, W. Sritrakool, Perfect self-similarity of energy spectra and gap-labeling properties in one-dimensional Fibonacci-class quasilattices, Phys. Rev. B 55 (5) (1997) 2882.
[27] L. He, X. Liu, G. Strang, Trees with Cantor eigenvalue distribution, Stud. Appl. Math. 110 (2) (2003) 123–138.
[28] C.N. Loong, E.G. Dimitrakopoulos, Recursive modal properties of fractal monopodial trees, from finite to infinite order, J. Sound Vib. 595 (2025) 118770.
[29] I.Z. Kostadinov, Fractal Hamiltonians in condensed matter physics, Phys. Scr. 36 (3) (1987) 516.
[30] B.D. Stosic, T. Stosic, I.P. Fittipaldi, J.J.P. Veerman, Residual entropy of the square ising antiferromagnet in the maximum critical field: the fibonacci matrix, J. Phys. A: Math. Gen. 30 (10) (1997) L331.
[31] D.E. Katsanos, S.N. Evangelou, Level-spacing distribution of a fractal matrix, Phys. Lett. A 289 (4) (2001) 183–187.
[32] W.J. Hsu, C.V. Page, J.S. Liu, Fibonacci cubes–A class of self-similar graphs, Fibonacci Quart. 31 (1) (1993) 65–71.
[33] E. Ferrand, An analogue of the Thue-Morse sequence, Electron. J. Comb. 14 (1) (2007) R30.
[34] J.C. Mason, D.C. Handscomb, Chebyshev Polynomials, CRC Press, 2002.
[35] A. Böttcher, S.M. Grudsky, Spectral Properties of Banded Toeplitz Matrices, SIAM, 2005.
[36] F.R.K. Chung, Spectral Graph Theory, vol. 92, American Mathematical Soc., 1997.
[37] O.O. Bendiksen, Flutter of mistuned turbomachinery rotors, J. Eng. Gas Turbines Power 106 (1) (1984) 25–33.
[38] O.O. Bendiksen, Localization phenomena in structural dynamics, Chaos Solitons Fractals 11 (10) (2000) 1621–1660.
[39] S.T. Wei, C. Pierre, Statistical analysis of the forced response of mistuned cyclic assemblies, AIAA J. 28 (5) (1990) 861–868.
[40] M.P. Mignolet, C.C. Lin, The combined closed form-perturbation approach to the analysis of mistuned bladed disks, J. Turbomach. 115 (4) (1993) 771–780.
[41] M.P. Mignolet, W. Hu, I. Jadic, On the forced response of harmonically and partially mistuned bladed disks. Part I: Harmonic mistuning, Int. J. Rotating Mach. 6 (1) (2000) 29–41.
[42] Z. Vargha, Comparison of Measured and Numerically Calculated Data of the Turbulent Flow Behind a Grid and Modelling Turbulence with a Mechanical Model (Master’s thesis), Budapest University of Technology and Economics, 2016.